Charged Black Hole Solutions in Alternative Theories of Gravity

A thesis
presented to the University Of Waterloo
in fulfilment of the
thesis requirement for the degree of
Master of Science
in
Physics and Astronomy

Waterloo, Ontario, Canada, 2016

This thesis consists of material all of which I authored or co-authored: see Statement of Contributions included in the thesis. This is a true copy of the thesis, including any required final revisions, as accepted by my examiners. I understand that my thesis may be made electronically available to the public.

Statement of Contribution

This dissertation is partially the product of collaborative research and co-authored publications as follows:

Chapter 1 Michael Meiers, Mehdi Saravani and Niayesh Afshordi, Cosmic Censorship in Lorentz Violating Theories of Gravity, *Phys. Rev.*, vol. D93, p.104008, 2016

Chapter 2 Forthcoming publication by Michael Meiers and Robert Mann. Based on work originally started by Luke Bovard.

Abstract

In my thesis, I examine charged black holes in two contexts. The first part covers the formation of something analogous to event horizons for a class of Lorentz-Violating theories which allow for signals to travel faster than light. In particular, the focus is put on the construction of horizons for the limiting case where the signal travels infinitely fast called a universal horizon. An explicit construction for a metric containing a massive collapsing charged shell is presented followed by an extension into rotating systems using a geometric argument. The latter context is Randall Sundrum model of gravity applied to higher dimensions. The research begins with a general ansatz and restricts parameter space using the equations of motion and junction conditions created by brane on which some charge is trapped. Some examination of the available solutions follows, and an analysis of the entropy relations for large and small black hole solutions concludes the results.

Acknowledgements

This research was supported by Natural Sciences and Engineering Research Council of Canada by the Province of Ontario through the Ministry of Research and Innovation. A special thanks is given to Niayesh Afshordi and Robert Mann for their mentorship and insight. An acknowledgement of the work done by Luke Bovard on his early work on the RS solutions is noted gratefully. Another thank you is given to Mehdi Saravani for his help and collaboration on the first half of this work.

Contents

List of Figures

List of Tables

Overview

The following is a collection of work conducted during my time as a Masters student a the University of Waterloo. Although the two independent projects are quite disparate in scope both broadly look at alternative theories of gravity and some of their consequences. Chapter 1 is the contents of published paper (1) that will cover the formation of universal horizons, a structure that will be explained below, first in the context of a collapsing charged massive shell, and then examining an eternal spinning system. Chapter 2 will address extremal Randall-Sundram black holes of arbitrary dimension and examine how the entropy of the bulk and brane systems are related.

The earlier chapter is motivated by models which contain a preferred frame such as k-essence, Cuscuton or Hořava-Lifshitz. K-essence is a special type of quintessence theory with a non-canonical kinetic term. Quintessence theory was proposed in (2) to attempt to solve part of the cosmological constant problem. The cosmological constant problem occurred because, despite changing at drastically different rates, matter and dark energy have the same scale of energy density throughout the universe in modern times. This coincidence is quite troubling, as when we only use Λ-CDM we would require the initial energy density of dark energy to be 100 orders of magnitude smaller than matter in the earlier universe. Because of this peculiarity, the problem is known as the cosmological coincidence problem (3). Quintessence theories attempt to solve this by having a scalar field which follows the energy density of radiation until radiation-matter equality where its behaviour changes to match dark energy. However, the non-canonical kinetic terms in K-essence, result in signals which can propagate faster than light. This property causes a lot of pause for those researchers concerned about causality. However in (4), we are assured that causality can be preserved by some metrics and those that do not would be considered physically unreasonable, much like how we consider metrics which would create close timelike curves in 4-D general relativity non-physical. If we take the speed at which these signals travel in k-essence and allow them to go infinitely fast, we lose dynamic degrees of freedom but gain constraints on the dynamic sector in such a way that creates behaviour like modified gravity(5). This limiting case is known as Cuscuton theory. It is an interesting limit to look at as it is also the low energy limit of the chief motivation for the first chapter, Hořava-Lifshitz gravity (6). Hořava-Lifshitz attempts to make progress in quantum gravity by fundamentally breaking the equivalence of time and space

at high energies. Because of this symmetry loss, Hořava-Lifshitz gravity features a singular foliation for a given geometry. All of these theories feature an action of the form the scalar field ϕ is

$$S = \int \mathrm{d}^4x\sqrt{-g}\mathcal{L}(X,\phi)$$

where $X = \frac{1}{2}g^{\mu\nu}\nabla_\mu\phi\nabla_\nu\phi$. The theories of interest have a Lagrangian density of the form

$$\mathcal{L} = aX^n - V(\phi)$$

which was concisely shown in (7) to have as speed of sound of

$$c_s^2 = \frac{1}{2n-1}$$

where $n \to \frac{1}{2}$ corresponds to Cuscuton and the low energy sector of Hořava-Lifshitz we are interested.

Following the lead of (7), we are interested in seeing if these theories can be applied to other classic black hole solutions. Signals which travel arbitrarily fast could cause problems for the idea of a shielded singularity. However, it has been seen that an analogous structure to an event horizon, called a universal horizon form for signals which could travel infinitely fast. This structure is then the limiting case for theories which feature superluminal but finite speeds of sounds. The focus primarily is to find this horizon for spherically symmetric charged collapsing shell. We will utilize the standard metric for this system and solve for the lines of constant time that are defined by the preferred frame. Some thoughts of how to extend the analysis to more general problems and an application to the classic Kerr solution are then presented.

In the second chapter we approach a horizon solution using a theory which was proposed to explain a different problem. The hierarchy problem of forces asks why gravity is comparatively so weak compared the forces which govern the standard model of particle physics. Lisa Randall and Raman Sundrum (RS) proposed in 1999 a mechanism which attempts to solve this problem (8). The initial mechanism had the standard model constrained to a brane inside a higher dimensional bulk. In the original mechanism the space was bookended by another brane where gravity would be strong. The model we are interested in only requires a single brane to where particles are restricted. This so called RS II model is especially interesting as it is an AdS bulk which has desirable physics on a codimension-1 subspace which might be of keen interest for those studying the AdS/CFT correspondence. A reconstruction of low energy RS II can be seen from this perspective in (9). RS II is able to recover perturbation Newtonian gravity at low energies for distances large compared to the bulk AdS radius. In order to see if this would be able to recover the known properties of general relativity, previous work has endeavoured to find black hole solutions. These have proven difficult to find but in 2009 Kaus and Reall(KR) found means to find extremally charged black hole solutions(10). In previous work before them (11), there had been found solutions which would require that RS's model inherently

takes account for quantum corrections to general relativity. If RS's model took account of these correction a static solution would be impossible to find bar for some specific cases. Hence their choice of extremally charged black holes. In the extreme limit the charged ReissnerNordstr om black hole has zero temperature, allowing for the restoration of an assumption of a static evolution.

Curious to see if these approaches are robust enough to be carried to higher dimensions, we take RS's second model and raise it up into higher dimensions. Following KR's approach, we start with the near horizon structure and attempt to solve the equations of motion for the full space. Israel junction conditions are imposed and the possible solutions are examined. Comparisons to the expected value from a higher dimensional Einstein-Hilbert action conclude the chapter.

Chapter 1

Universal Horizons in Charged and Spinning Spacetimes

1.1 Introduction

The theory of general relativity (GR) has been successful in describing a wide range of phenomena, from solar system to cosmological scales. In addition to being consistent with various experiments, the mathematical elegance of the theory is very appealing. Diffeomorphism invariance, at the core of GR, gives a straightforward constructive way of building the theory.

From an observational point of view, there is no reason to abandon this theory. GR is compatible with a wide variety of experimental constraints[1]. On the other hand, many attempts have shown so far that modifying GR is a tricky task, and one often faces physically unacceptable results, e.g. the appearance of the Boulware-Deser ghost in massive gravity (12) and ghost degrees of freedom in quadratic gravity (13).

However, studying non-GR theories of gravity is still valuable, and the main reason stems from quantizing gravity. GR, while being a very successful classical theory, has failed to cope with quantum mechanics. Therefore, one approach to quantum gravity has been to abandon diffeomorphism invariance, as e.g., done in the celebrated Horava-Liftshitz gravity (14). However, the strict empirical constraints on violations of the equivalence principle requires observable deviations from Lorentz symmetry to be limited to high energies, which provides a challenge for the construction of these theories (e.g., (15)).

[1] Although there have been various attempts to solve the problems of dark matter and dark energy with GR modifications, simple solutions to these problem in the context of GR exist. In other words, there is no apparent observational contradiction with GR which necessitates GR modifications.

In different examples of theories with broken Lorentz invariance, superluminal degrees of freedom appear (see (16; 17)). The existence of superluminal excitations (SLE) points out that a different causal structure exists in these theories compared to GR, even when the back-reaction of these excitations on the geometry is negligible. This property is especially significant for black hole (BH) solutions. While potentially SLE can escape the traditional Killing horizon of a BH and make the classical theory unpredictable (18), it has been shown in many examples (19; 20; 21; 22; 23; 24; 25; 26) that a notion of horizon (called universal horizon) still exists in these theories. Moreover, universal horizons (UH) thermally radiate and satisfy the first law of horizon thermodynamics[2] (27; 28; 29; 30) (but also see (31)). Studying the notion of universal horizons and its temperature and entropy is important since it guides us to better understanding the structure of the UV theory.

In this chapter, we study the universal horizon formation in dynamical or stationary spacetimes with an inner killing horizon, in the limit of infinite sound speed for excitations (i.e. *incompressible* limit). In order to do so, we make use of the fact that surfaces of global time (defined by the background field), in the incompressible limit of Lorentz violating theories, coincide with constant mean curvature (CMC) surfaces of the spacetime (6). Furthermore, the backreaction of the incompressible field on the spacetime geometry is negligible as long as the event horizon is much smaller than the cosmological horizon (7). In the next section, we show how the universal horizon forms in a dynamical setting, in the collapse of a charged shell, and we derive a formula for the radius of the universal horizon in terms of the charge. In Section 1.3.1, we propose a geometric definition for universal horizons. This allows us to study the universal horizon for spinning black holes. In 1.3.2, we show that there are three axisymmetric surfaces that satisfy the conditions of a universal horizon. This means that two families (with infinite numbers) of axi-symmetric universal horizons in the Schwarzschild case exist. Section 1.4 concludes the chapter.

1.2 Universal Horizon in Dynamic Reissner–Nordstrom Geometry

We start this section by finding CMC slicing of dynamic Reissner–Nordstrom (RN) geometry. As mentioned earlier, CMC surfaces of this spacetime are the constant global time surfaces of the background incompressible field, and they define the new causal structure imposed by this field (see the analysis in (7)). Once we derive the CMC slicing, we focus on the (universal) horizon formation in this geometry.

[2] so far only for spherically symmetric solutions

1.2.1 CMC Surfaces in a Dynamic Reissner–Nordstrom Geometry

In order to examine the formation of the universal horizon in a dynamic Reissner–Nordstrom geometry, one must first describe surfaces of constant mean curvature for a collapsing charged massive spherical shell. An examination of CMC surfaces has been similarly looked at in the restricted case of maximal surfaces ($K = 0$) (32). The dynamics of the collapse itself is well known and described by Israel (33). Describing the metric in the standard way has the geometry inside the shell as flat and the RN spacetime outside. We write this geometry as:

$$\begin{aligned} \mathrm{d}s^2 &= f_-(r)\mathrm{d}t_-^2 - f_-(r)^{-1}\mathrm{d}r^2 - r^2\mathrm{d}\Omega^2 \qquad (r < R) \\ \mathrm{d}s^2 &= f_+(r)\mathrm{d}t_+^2 - f_+(r)^{-1}\mathrm{d}r^2 - r^2\mathrm{d}\Omega^2 \qquad (r > R) \end{aligned}$$

where $f_-(r) = 1$ and $f_+(r) = 1 - \frac{2M}{r} + \frac{Q^2}{r^2}$ in $G = c = 1$ units. The parameters are the gravitational mass M and shell's charge Q. For simplicity we will often use relative charge $q = Q/M$. While the spherical coordinates are shared between the inner and outer regions, the time coordinates t_- and t_+ correspond to the Minkowski and RN time respectively.

Let the family of spacelike CMC surfaces be denoted by $\Sigma_K(t_g)$ where t_g is a global time coordinate that is constant for each surface. The timelike normal vector to this surface is labelled v^μ. The CMC condition implies $\nabla_\mu v^\mu = K$, resulting in:

$$\frac{\partial}{\partial t_\pm} v^{t_\pm} + \frac{1}{r^2}\frac{\partial}{\partial r} r^2 v^r = K \tag{1.1}$$

If we denote $B \equiv -r^2 v^r$ and use the normalization condition $v_\mu v^\mu = 1$ then:

$$r^2 v^{t_\pm} = \pm f_\pm(r)^{-1}\sqrt{B^2 + f_\pm r^4}. \tag{1.2}$$

For now we use the '+' case so that $v_t > 0$ for $r \gg M$. Additional explanation and the cases where '−' is relevant will be seen in Section 1.2.4. Combining this result with (1.1) we get

$$\frac{B}{f_\pm(r)\sqrt{h(r,B)}}\frac{\partial}{\partial t_\pm} B - \frac{\partial}{\partial r} B = K r^2 \tag{1.3}$$

with $h(r, B) = B^2 + f_\pm r^4$. The characteristic equations of (1.3) are simply:

$$\frac{\mathrm{d}t_\pm}{\mathrm{d}s} = \frac{B}{f_\pm(r)\sqrt{h(r,B)}}, \quad \frac{\mathrm{d}r}{\mathrm{d}s} = -1, \quad \text{and} \quad \frac{\mathrm{d}B}{\mathrm{d}s} = K r^2, \tag{1.4}$$

for some parameter s. Using the second equation of (1.4) to integrate the first and third equations results in:

$$t_\pm = (t_\pm)_0 - \int_{r_0}^{r} \frac{B\mathrm{d}r}{f_\pm(r)\sqrt{h(r,B)}}, \quad \text{and} \quad B = \frac{K}{3}(r^3 - r_0^3) + B_0, \tag{1.5}$$

where $(t_\pm)_0$, r_0, and B_0 are integration constants. In order to fix these constants, we examine the internal and external cases separately.

1) Inside the shell: If $r_0 = 0$ then $B(r = 0) = B_0$. If $B_0 \neq 0$ this would lead to a contradiction, as $v^r = \frac{-B}{r^2}$ should be finite in the flat geometry. Therefore with $r_0 = 0$, the equation reduces to:

$$t_- = (t_-)_0 + \int_0^r \frac{Kr^3 \mathrm{d}r}{3\sqrt{(\frac{Kr^3}{3})^2 + r^4}} \text{ and } B = \frac{K}{3}r^3 \tag{1.6}$$

2) Ouside the shell: Let $r_0 = R((t_+)_0)$. We can determine B_0 by looking at the boundary between the flat and RN spaces. Projecting the vector v^μ along the shell should give us continuous observable values. The shell's timelike path comes from $S = R(t_\pm) - r = 0$ which creates the unit normal vector and tangent vector labelled as n^μ and u^μ respectively. If we choose the sign of the normalization factors such that $u^r < 0$, the vectors take the form:

$$n^\mu_- = \frac{g^{\mu\nu}}{N_-}(\nabla_-)_\nu S = \frac{1}{N_-}(\frac{\mathrm{d}R}{\mathrm{d}t_-}, 1, 0, 0), \tag{1.7}$$

$$u^\mu_- = \frac{1}{N_-}(1, \frac{\mathrm{d}R}{\mathrm{d}t_-}, 0, 0), \tag{1.8}$$

$$N^2_- = 1 - (\frac{\mathrm{d}R}{\mathrm{d}t_-})^2, \tag{1.9}$$

inside the shell, while outside takes the form:

$$n^\mu_+ = \frac{g^{\mu\nu}}{N_+}(\nabla_+)_\nu S = \frac{1}{N_+}(f_+^{-1}\frac{\mathrm{d}R}{\mathrm{d}t_+}, f_+, 0, 0), \tag{1.10}$$

$$u^\mu_+ = \frac{1}{N_+}(1, \frac{\mathrm{d}R}{\mathrm{d}t_+}, 0, 0), \tag{1.11}$$

$$N^2_+ = \frac{f_+^2 - (\frac{\mathrm{d}R}{\mathrm{d}t_+})^2}{f_+}. \tag{1.12}$$

We wish to find functions $C(R)$ and $D(R)$, such that:

$$v^\mu_- = Cn^\mu_- + Du^\mu_-. \tag{1.13}$$

From inside the shell $v^\mu(R) = (1, 0, 0, 0)$ which means $C = \frac{-1}{N_-}\frac{\mathrm{d}R}{\mathrm{d}t_-}$ and $D = \frac{1}{N_-}$. Requiring projections (C and D) to match at the boundary, we get:

$$B_0 = -R^2(C(n_+)^r + D(u_+)^r) = \frac{R^2}{N_+N_-}\left(\frac{\mathrm{d}R}{\mathrm{d}t_+} - f_+\frac{\mathrm{d}R}{\mathrm{d}t_-}\right). \tag{1.14}$$

So, if we specify the dynamics of the shell $\frac{dR}{dt_\pm}$, all the parameters are fixed.

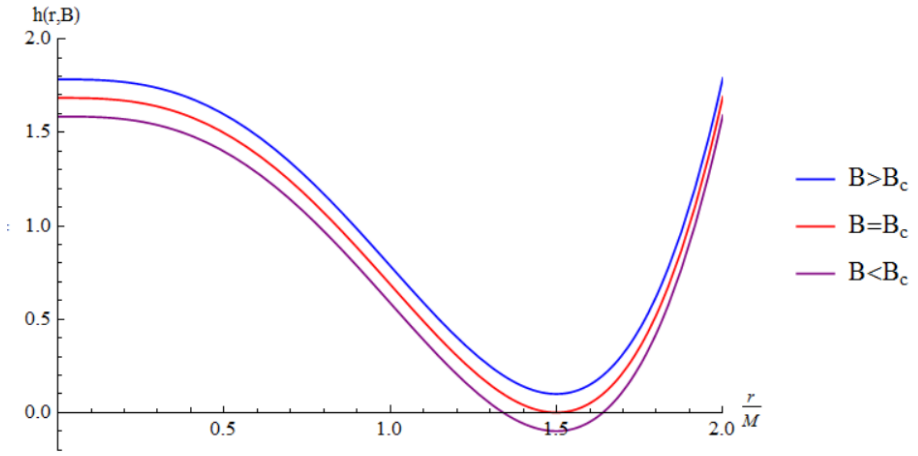

Figure 1.1: $h(r, B)$ with sub-critical, post-critical and critical B for $Q = 0$.

The description of the radial velocity comes from Israel and De La Cruz (33):

$$\left(\frac{\mathrm{d}R}{\mathrm{d}t_-}\right)^2 = 1 - \frac{R^2}{(\epsilon R - b)^2}, \tag{1.15}$$

$$\left(\frac{\mathrm{d}R}{\mathrm{d}t_+}\right)^2 = f_+^2 - \frac{f_+^3 R^2}{(\epsilon R - b - \frac{m}{\epsilon})^2}, \tag{1.16}$$

where $\epsilon = \frac{M}{\mathcal{M}}$ and $b = \frac{M(\epsilon^2 q^2 - 1)}{2\epsilon}$ with $\mathcal{M}$ denoting the total rest mass. We can use (1.15) and (1.16) to reduce $N_+ = \frac{R f_+}{\epsilon R - b - \frac{M}{\epsilon}}$ and $N_- = \frac{R}{\epsilon R - b}$. Note that N_+ changes signs to enforce $u^r < 0$, becoming negative only when $\frac{\mathrm{d}R}{\mathrm{d}t_\pm}$ flips signs. These choices simplifies B_0 to:

$$B_0 = \frac{M}{\epsilon}\sqrt{(\epsilon R - b)^2 - R^2}. \tag{1.17}$$

1.2.2 Horizon Formation

Following the analysis of (7), we examine the properties of t_+. The behaviour of t_+ heavily depends on $h(r, B)$. While B is large, which corresponds to large R, $h(r, B)$ is never vanishing. However when a critical value B_c is reached, $h(r, B_c)$ has double root at a particular value of r labelled r_h (see Figure 1.1). Something interesting will occur when r_h is larger than the radius of the shell for which B_c occurs, named R_{lc} or the radius of *last contact* ($B(R_{lc}) = B_c$). A signal sent out from the shell at R_{lc} will proceed out to r_h but takes infinitely long time to ever reach this radius. In fact, signals sent just outside R_{lc} will

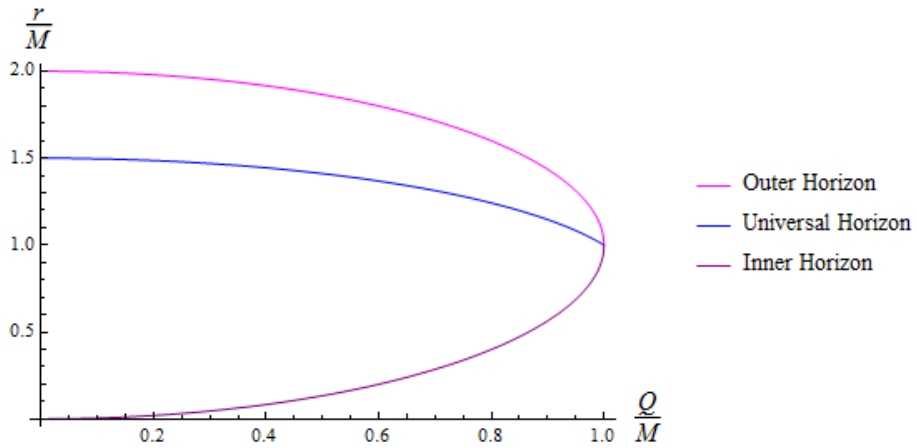

Figure 1.2: The outer, inner, and universal horizons for $K = 0$ and varying Q

form an envelope around r_h staying at this radius longer and longer, as R_{lc} is approached, before escaping to infinity (see Figure 1.3). The values of B_c and r_h can be found by finding the solutions to $h(r, B) = \frac{\partial h(r,B)}{\partial \mathrm{r}} = 0$. We examine this equation in two different cases.

Case 1: $K = 0$

Equations for the double root reduce to:

$$r_h^4 - 2Mr_h^3 + Q^2 r_h^2 + B_c^2 = 0 \tag{1.18}$$
$$2r_h^3 - 3Mr_h^2 + Q^2 r_h = 0 \tag{1.19}$$

to which the solutions with non-negative real B_c are the trivial $r_h = B_c = 0$ and

$$r_h = \frac{3M}{4} + \frac{M}{4}\sqrt{9 - 8q^2} \tag{1.20}$$
$$B_c = r_h\sqrt{-r_h^2 + 2mr_h - Q^2} = r_h^2\sqrt{-f_+(r_h)}. \tag{1.21}$$

It is of interest to note that the asymptotic radius of the UH is always between the inner and outer killing horizons of the metric (see Figure 1.2).

Case 2: $K \neq 0$

Equations for the double root are written as:

$$\frac{K^2}{9}r_h^6 + r_h^4 + (\frac{2KB_c}{3} - 2M)r_h^3 + Q^2 r_h^2 + B_c^2 = 0,$$
$$\frac{K^2}{3}r_h^5 + 2r_h^3 + (KB_c - 3M)r_h^2 + Q^2 r_h = 0.$$

The non-trivial solution for B_c is:

$$B_c = r_h\sqrt{-r_h^2 + 2Mr_h - Q^2} - \frac{Kr_h^3}{3} = r_h^2\sqrt{-f_+(r_h)} - \frac{Kr_h^3}{3}, \tag{1.22}$$

however as B_c is dependant on r_h the solution for r_h must be perturbatively expanded in K. To linear order the solution is:

$$r_h = r_h^0 - K\frac{(r_h^0)^3\sqrt{-f_+(r_h^0)}}{M\sqrt{9-8q^2}} + \mathcal{O}(K^2), \tag{1.23}$$

where $r_h^0 = \frac{3M}{4} + \frac{M}{4}\sqrt{9-8q^2}$. Assuming that the expansion of the background field is negligible (for example fixed by cosmology, as $K = 3\times$Hubble constant), in the region of interest $0 < r < 2M$ the effect of terms containing K are insignificant. From here we set $K = 0$ as its effect will only come into play when looking at the causal structure when R is very large.

The last unknown of the universal horizon is where it begins before it asymptotes to r_h. To solve for R_{lc} we use that $B(R_{lc}) = B_c$ and it results in either:

$$R_{lc} = \frac{b}{2} - \frac{B_c^2}{2bM^2}, \tag{1.24}$$

for $\epsilon = 1$ or

$$R_{lc} = \frac{\epsilon b + \sqrt{\epsilon^2(\epsilon^2-1)B_c^2/M^2 + b^2}}{\epsilon^2 - 1}, \tag{1.25}$$

for $\epsilon > 1$.

We take the larger of the solutions to the quadratic, as the first instance of B_c will create the behaviour desired.

1.2.3 Inside the Universal Horizon

The foliation can be extended for $B < B_c$, however some subtleties arise. Denote the unit tangent vector of the CMC surfaces at the point the surface intersects the shell as s^μ which in components can be written as:

$$s^\mu = \frac{1}{N_s}(T'_{cmc}(R), 1, 0, 0), \tag{1.26}$$

$$N_s^2 = \frac{1 - f_+^2 T'^2_{cmc}}{f_+} = \frac{R^4}{h(R, B(R))}, \tag{1.27}$$

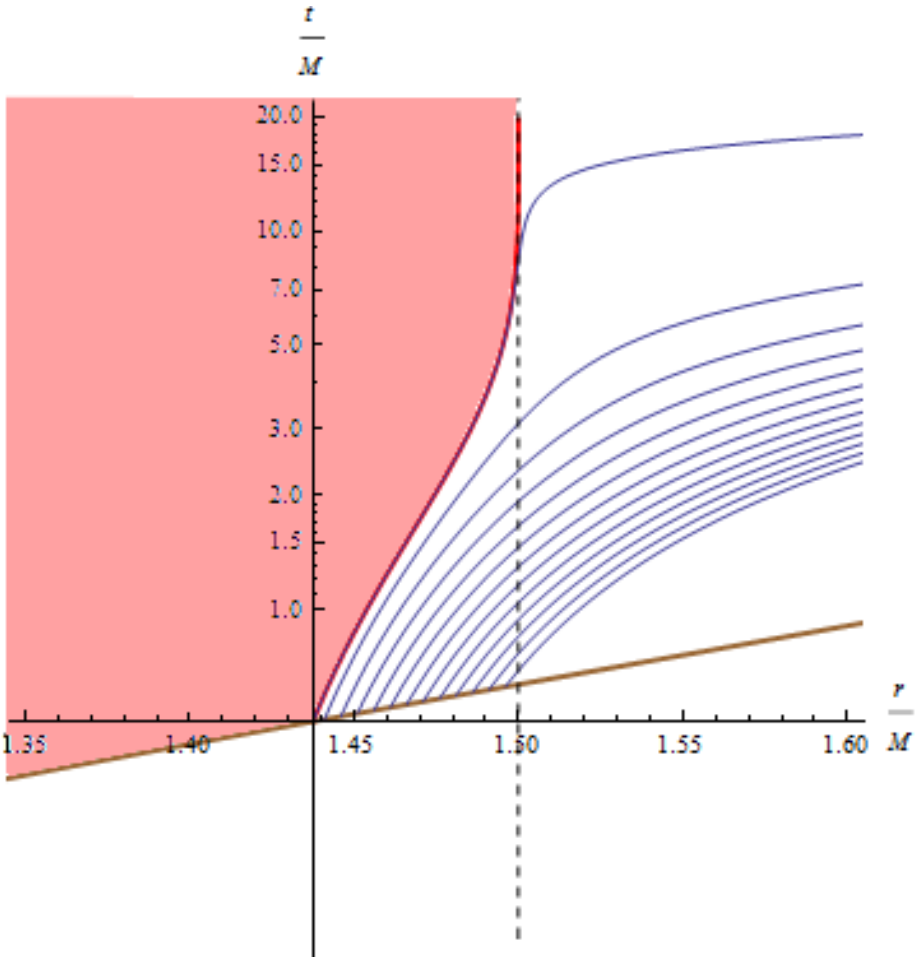

Figure 1.3: The universal horizon formation for $Q = 0$ in Schwarzschild coordinates. The blue lines represent CMC surfaces, the lowest brown line where the CMC lines originate from is the shell's surface, the red line and the boundary of the shaded region is the universal horizon (UH).

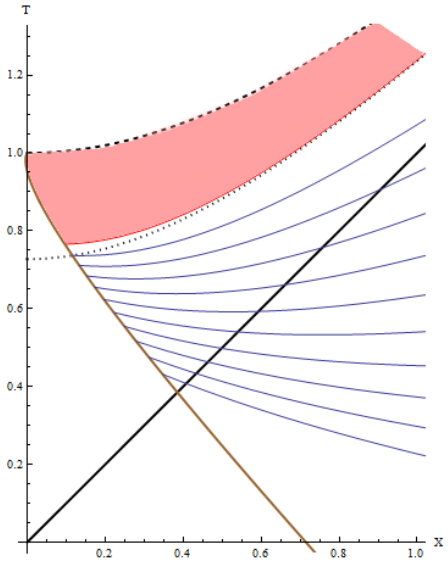

(a) The universal horizon formation for $Q = 0$ in Kruskal-Szekeres coordinates. The lines/region have the same meaning as Figure 1.3, additionally ,the dotted black is the radius that UH asymptotes to, the thick black line represents the null horizons, and the dashed line the singularity.

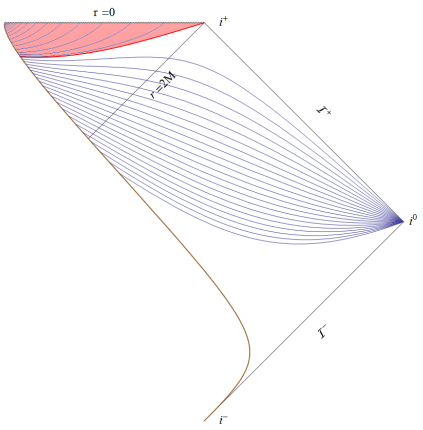

(b) The Penrose diagram for a $Q = 0$ collapsing shell depicting the UH horizon. The lines/region have the same meaning as Figure 1.3 with the inclusion of sub-UH CMC surfaces in blue.

Figure 1.4: Surfaces for constant global time and formation of the universal horizon in Kruskal-Szekeres coordinates and Penrose diagram for $Q = 0$.

where the last equality comes from using the derivative of (1.5). In general $h(r, B(R))$ is a quartic that can not easily be factored, however when restricted to the surface of the shell it can be factored to:

$$h(R, B(R)) = \left(R^2 - MR + \frac{Mb}{\epsilon}\right)^2. \tag{1.28}$$

Thus one can write the normalization factor as:

$$N_s = \frac{R^2}{R^2 - MR + \frac{Mb}{\epsilon}}. \tag{1.29}$$

As a result, between the zeroes of $1/N_s$ at $M\frac{1\pm\sqrt{1-4b/\epsilon}}{2}$ we get $s^r < 0$. In particular this means that rather than increasing in r the CMC surfaces that intersect between these two roots will have a strictly decreasing r coordinate. Moreover it is precisely at these points where s^t switches signs corresponding to the second solution for T'_{cmc} which comes from the '-' solution to $r^2 v^{t_+}$.

The second complication occurs when R does not lie between the roots of N_s while still being less than R_{lc}. Here the CMC surface increases its radial coordinate initially only to encounter a zero of $h(r, B(R))$ at r_{turn}. The integral for t_+ can carried out since T'_{cmc} only depends on the square root of $h(r, B(R))$ and, by construction, r_{turn} is only a first order zero of $h(r, B(R))$. After this point T'_{cmc} switches signs and the r coordinate begins decreasing, flipping the direction of the integration taking the surface from r_{turn} to 0.

Now that these subtleties are understood, we are ready to examine the structure of the complete foliation.

1.2.4 Foliation Structure

We will break up the discussion into several sections. For all our analysis we consider the shell to be dropped from infinity thus $\epsilon \geq 1$ (33), in particular the inward velocity of the shell at infinity is exactly $\sqrt{\epsilon^2 - 1}$. There are 4 cases of interest:

Case 1: $Q = 0$

When restricted to Schwarzschild, $b = \frac{-M}{2\epsilon}$ making it strictly negative. In particular the value of ϵ is only relevant to the radius of last contact, and so without losing any depth of examination we set $\epsilon = 1$. Figures 1.3 and 1.4a illustrate the foliations created by the CMC surfaces for $R > R_{lc}$ and the final well defined CMC surface that creates the universal horizon in Schwarzchild and Kruskal-Szekeres coordinates. Once a conformal compactification has been performed the casual structure is clear in Figure 1.4b with the additional sub-UH CMC surfaces (which end in a singularity, rather than the space-like infinity i^0).

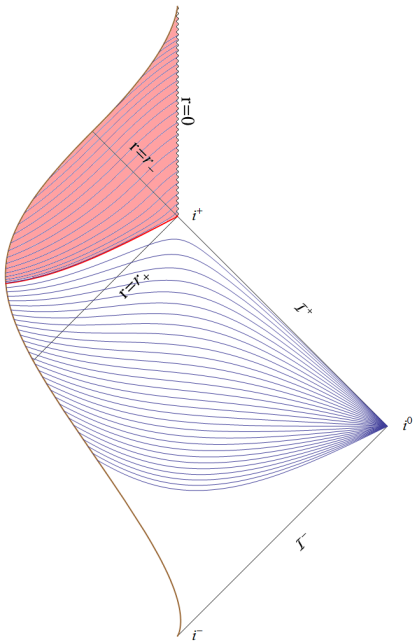

Figure 1.5: The Penrose diagram for $Q = 0.99M$ and $\epsilon = 1$ collapsing shell depicting the UH. The lines/region have the same meaning as Figure 1.3 with the inclusion of sub-UH CMC surfaces in blue.

Case 2: $Q \neq 0$ **&** $b \leq 0$

For ϵ small enough such that the numerator of b remains negative, the shell is unable to rebound before collapsing to a singularity. Schwarzchild and the charged generalization of Kruskal-Szekeres remain almost identical in their analogous charts. The causal structure in Figure 1.5 reveals the distinction from case 1. The collapse ends in the coordinates, colloquially called the *parallel universe*.

Case 3: $Q \neq 0$ **&** $0 < b < b/\epsilon + 1/\epsilon^2$

For the range of ϵ such that $0 < b < \frac{M}{\epsilon^2}$, the shell rebounds at the radius of $\frac{b}{\epsilon-1}$ but in the parallel coordinates that distinguish it from the next case. In particular this means that $t(R)$ has a stationary point between r_+ and r_-. Figure 1.6 shows the collapse and the corresponding causal structure for this case.

Case 4: $Q \neq 0$ **&** $b \geq b/\epsilon + 1/\epsilon^2$

Subsequently for $b > \frac{M}{ep}$ shell rebounds at the radius of $\frac{b}{\epsilon-1}$ in the original coordinate charts or exactly where the original and parallel coordinates meet .

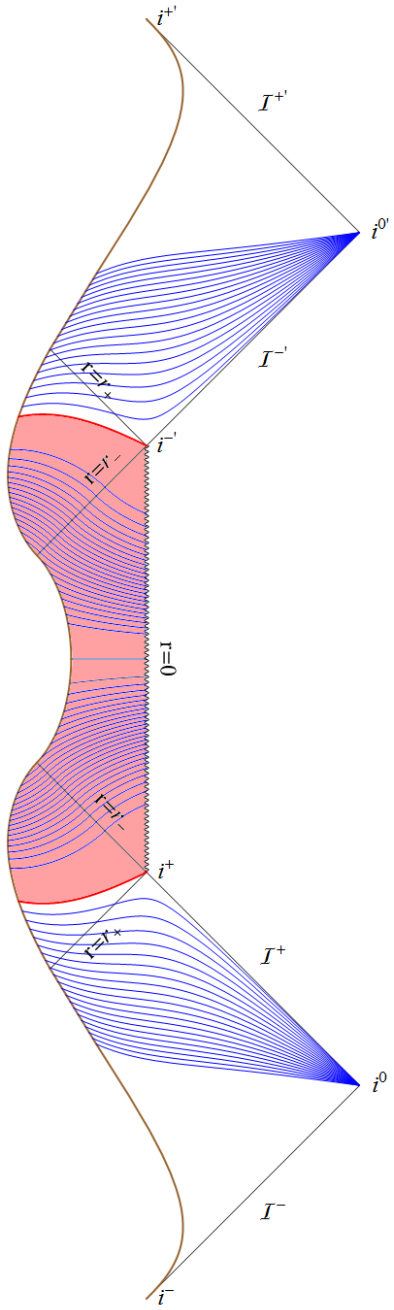

Figure 1.6: The Penrose diagram for $Q = 0.99M$ and $\epsilon = 1.1$ values. These parameters make $b/(\epsilon-1) < b/\epsilon+1/\epsilon^2$. The lines/region have the same meaning as Figure 1.3 with the inclusion of sub-UH CMC surfaces in blue.

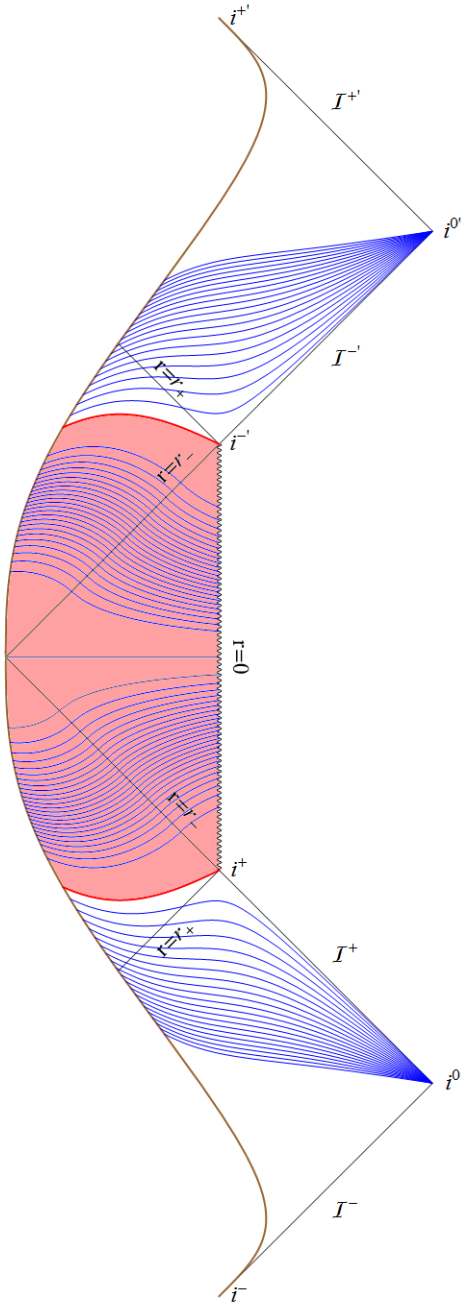

Figure 1.7: The Penrose diagram for $Q = 0.99M$ and ϵ set to make $b/(\epsilon - 1) = b/\epsilon + 1/\epsilon^2$. The lines/region have the same meaning as Figure 1.3 with the inclusion of sub-UH CMC surfaces in blue.

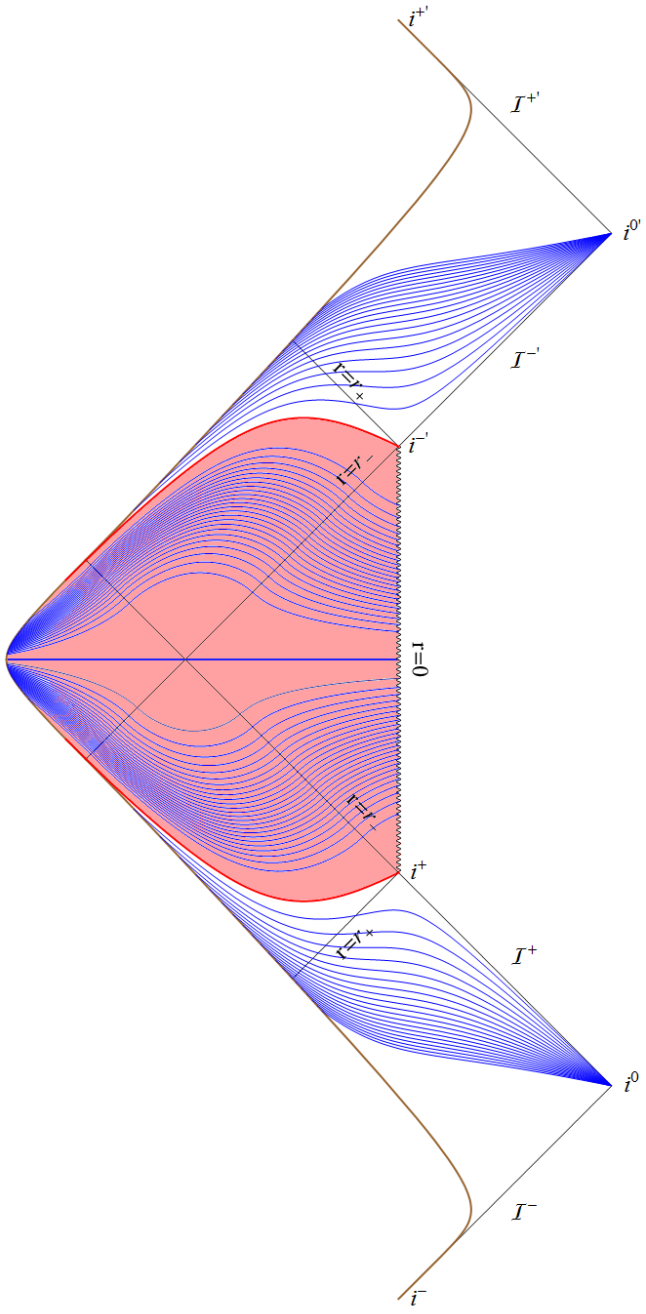

Figure 1.8: The Penrose diagram for $Q = 0.99M$ and $\epsilon = 3/2$ values. These parameters make $b/(\epsilon - 1) > b/\epsilon + 1/\epsilon^2$. Coloured lines/region have the same meaning as Figure 1.3 with the inclusion of sub-UH CMC surfaces in blue.

In particular this means that $t(R)$ has a stationary point at or inside r_-. The Schwarzchild and Kruskal-Szekeres coordinates are again nearly indistinguishable from case 1 except when the placement of R_{lc} requiring that the UH being in a second charts however this does not reveal any new structure. Figure 1.7 and 1.8 represents paths within this case, $b = b/\epsilon + 1/\epsilon^2$ and $b > b/\epsilon + 1/\epsilon^2$ respectively. In this final case $R_{lc} < r_-$ resulting in the the UH piercing the r_-. Nevertheless, the singularity and the parallel interior horizon, which is considered to be unstable (34) is still hidden within the UH.

1.2.5 Censorship in Reissner-Nordstrom

Ultimately, in all the above cases, the UH shields any singularity from being probed even using superluminal signals and preserves a sense of cosmic censorship in Lorentz violating theories. It is apparent from the structure that every CMC is terminated at i^0, i^+, $i^{-\prime}$,$i^{0\prime}$ or the singularity. We would posit an analogous, although informally made, statement to the original *weak* cosmic censorship conjecture: the set of points which can be connected to i^0 with CMC surfaces (an analogous property of being in the causal past of $\mathcal{I}^+$) is distinct from the set of points which can be connected to the singularity. Moreover, the boundary between these two sets will exactly be the universal horizon.

Even though we have plotted the maximal foliation of spacetime beyond the universal horizon, one can argue that the self-consistent evolution of the Lorentz-violating theory (including, e.g., backreaction or quantum effects, which we have ignored) stops at the universal horizon, which can be viewed as the boundary of classical spacetime (see Sec. VI in (7) for more discussions).To see this more explicitly, note that the CMC surfaces beyond universal horizon end in singularity. Therefore, arbitrarily fast communication along these surfaces leads to a breakdown of initial value formulation in this region. The fact that both curvature singularity and the (potentially unstable) inner killing horizon (34) lie beyond the universal horizon, further suggests a notion of *strong* cosmic censorship.

Note that in the cases where a parallel universe exists, a second UH acts as a white hole horizon for superluminal signals.

1.3 Spinning Black Holes: A Tale of Three Horizons

1.3.1 Geometrical Definition of Universal Horizon

In the previous section, we discussed the formation of universal horizon in a dynamic RN geometry. Before moving on to the spinning black hole case, it would be illuminating to acquire more intuition about the geometric nature of the universal horizon. We start by asking the following question: is there a way of finding the universal horizon in the final geometry (after collapse completed) without knowing the details of collapse?

Let's consider the Schwarzschild case ($Q = 0$ collapse). CMC surfaces in the thin shell collapse geometry describe the surfaces of constant global time. As we discussed earlier, as long as we are interested in the behaviour of these surfaces near the black hole (small radii) we can treat them as maximal surfaces ($K = 0$). Maximal surfaces in this geometry inside the Schwarzschild radius asymptote to $r = \frac{3}{2}M$ before escaping to infinity. This suggests that $r = \frac{3}{2}M$ itself should be a maximal surface. In fact, one can simply verify that $r = r_*$ is a maximal (space-like) surface in Schwarzschild spacetime, only if $r_* = \frac{3}{2}M$.

This observation suggests a geometrical definition for an (asymptotic) universal horizon in stationary spacetimes; it is a maximal space-like hypersurface which is invariant under the flow of a time-like killing vector. Let's discuss each element of this definition.

First of all, a UH has to be a maximal surface as we described earlier. It also has to be space-like, since it describes a constant global time surface. Secondly, it is invariant under time translation, as it is the asymptotic surface of the maximal slicing.

We will show later explicitly that this definition does not pick a unique hypersurface. However, this should not be surprising, since the position of universal horizon depends on the behaviour of the background incompressible fluid (which defines the global time), unlike the killing horizon where its position is independent of the behaviour of the background fields (7; 4). Again, let's consider Schwarzschild spacetime. If we use the given definition of UH *with the additional assumption of spherical symmetry*, there is a unique solution of $r = \frac{3}{2}M$. However, there are many non-spherical UHs in the same geometry.

Before moving to the spinning case, let's find the spherical UH of RN geometry using the definition given above. Assume $r = r_h$ to be the universal horizon and v_μ the unit normal vector to this surface. Solving

$$\nabla_\mu v^\mu = 0, \tag{1.30}$$

we get

$$f'(r_h) = -4f(r_h), \tag{1.31}$$

with $f(r) = 1 - \frac{2M}{r} + \frac{Q^2}{r^2}$. Eq. (1.31) has a unique solution, which coincides with our previous result for a universal horizon (1.20), and is plotted in Figure (1.2). One can also directly check that (1.31) is equivalent to system of equations (1.18) and (1.19).

1.3.2 Universal Horizon in Kerr geometry

In this section, we find the asymptotic universal horizon of the Kerr metric. Given our definition above, it is a static axisymmetric[3] (space-like) maximal

[3]we assume that the background incompressible field obeys the axial symmetry of Kerr geometry.

surface. We express the Kerr metric in the following coordinates:

$$\begin{aligned} ds^2 = & \left(1-\frac{2mr}{\rho^2}\right)dt^2 - \frac{\rho^2}{\Delta}dr^2 - \rho^2 d\theta^2 - \frac{4mra\sin^2\theta}{\rho^2}dtd\phi \\ & - \left(r^2+a^2+\frac{2mra^2\sin^2\theta}{\rho^2}\right)\sin^2\theta d\phi^2 \end{aligned} \tag{1.32}$$

where

$$\rho^2 = r^2 + a^2\cos^2\theta, \tag{1.33}$$
$$\Delta = r^2 - 2mr + a^2. \tag{1.34}$$

The inner (r_-) and outer (r_+) killing horizons are the solution to $\Delta = 0$.

UH is the surface

$$r = r_h(\theta) \tag{1.35}$$

which satisfies

$$\nabla_\mu v^\mu = 0 \tag{1.36}$$

where v^μ is the (time-like) normal vector to the universal horizon. In other words,

$$v_\mu = \frac{1}{N}(0, 1, -r_h', 0) \tag{1.37}$$

where $'$ is the derivative w.r.t θ and N is the normalization factor

$$N^2 = -\frac{1}{\rho^2}\left(\Delta + r_h'^2\right). \tag{1.38}$$

Equation (1.38) leads to the following conclusion: demanding the UH to be a space-like surface (v^μ to be time-like) requires the UH to be positioned between the inner and the outer killing horizons

$$N^2 > 0 \to \Delta < 0 \to r_- < r_h(\theta) < r_+. \tag{1.39}$$

Now on to finding $r_h(\theta)$: Equation (1.36) takes the form

$$\begin{aligned} & 2(r_h - m) + \tfrac{r_h(r_h^2-2mr_h+a^2)}{r_h^2+a^2\cos^2\theta} - \tfrac{(r_h-m)(r_h^2-2mr_h+a^2)}{r_h^2-2mr_h+a^2+r_h'^2} \\ & = \tfrac{r_h'}{\tan\theta} + r_h'' - r_h'\left[\tfrac{a^2\sin\theta\cos\theta}{r_h^2+a^2\cos^2\theta} + \tfrac{r_h'r_h''}{r_h^2-2mr_h+a^2+r_h'^2}\right]. \end{aligned} \tag{1.40}$$

One way to find the solution of this differential equation is to expand $r_h(\theta)$ in powers of a

$$r_h(\theta) = m\sum_{n=0}\frac{a^n}{m^n}r^{(n)}(\theta) \tag{1.41}$$

and solve the differential equation order by order. At zero order ($a = 0$), we expect $r^{(0)} = \frac{3}{2}$. At any higher order, we find a Legendre differential equation.

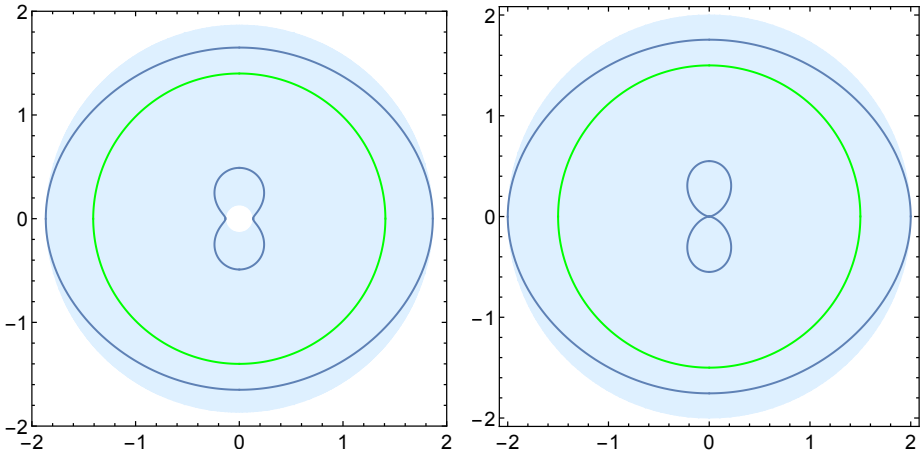

(a) $a = \frac{m}{2}$ (b) $a = 0$ (Schwarzschild)

Figure 1.9: Polar plot $\frac{r(\theta)}{m}$. Green curve is the UH solution of (1.41). Blue curves are additional numerical solutions to (1.40) and shaded region is the region between inner and outer killing horizons. The outer (inner) UH is tangent to the outer (inner) killing horizon at $\theta = \frac{\pi}{2}$.

Requiring a finite solution at $\theta = 0$ and $\theta = \pi$, this gives us a unique solution at any order. Here is the solution up to the order a^4:

$$\begin{aligned} r^{(2n-1)} &= 0, \quad n \in \{1, 2, \cdots\} \\ r^{(0)} &= \frac{3}{2} \\ r^{(2)} &= -\frac{1}{36}\cos^2\theta - \frac{13}{36} \\ r^{(4)} &= \frac{49}{10692}\cos^4\theta + \frac{29}{4752}\cos^2\theta - \frac{1057}{14256}. \end{aligned}$$

Surprisingly though, upon solving (1.40) numerically, we have found two more solutions that are different from (1.41) and do not approach to $r_h = \frac{3}{2}m$ as $a \to 0$ (see Figure 1.9).

The case of $a = 0$ is interesting, since the background geometry is spherically symmetric, and yet we have found two axisymmetric UHs. Moreover, we can always perform a rotation and get two other axisymmetric UHs. This means that there are two families (with infinite number in each family) of axisymmetric UHs in Schwarzschild spacetime.

1.4 Conclusion

In the incompressible (or infinitely fast propagation speed) limit of many Lorentz-violating theories of gravity, surfaces of constant mean curvature define the pre-

ferred foliation (7) (for a careful study of theories with infinite sound speed see (22)). For such theories, one may worry that superluminal signal propagation may lead to naked singularities. In this chapter, we have shown that a *universal* horizon always forms when a charged spherical shell collapses to form a Reissner–Nordstrom black hole. Evidence that causal horizon formation will take place in Lorentz-violating theories supports a conjecture similar to cosmic censorship in General Relativity.

We see that the universal horizon acts almost like an extension of i^+, since any observer approaching the UH will pass through all future CMC surfaces outside the UH. Consequently, the analysis conducted here is likely only valid in the classical regime (ignoring quantum effects like the evaporation of black holes). As a result the region close to the UH is potentially where non-classical effects will begin to become relevant. Making claims past this region may require the full UV theory or a closer examination of the classical consequences of Lorentz violating theories.

We have also presented a geometric definition for the UH which provides a tool for finding generic solutions in non-spherically symmetric geometries. This tool is additionally valuable as the full evolution of the system up to the point of UH formation is not needed to be explored. In particular, we show how the definition can be applied to the Kerr geometry, revealing a family of solutions in a non-spherical geometry.

Slowly rotating black hole solutions of Einstein-Aether theory have been studied in (35). Specifically, in the limit that the spin-0 mode of an Aether propagates infinitely fast, slowly rotating black hole solutions of Einstein-Aether and Horava-Lifshitz are the same and they possess a universal horizon. Corrections to the location of the universal horizon do not appear in the first order of rotation parameter (Equation (104) in (35)) which is consistent with our result in the previous section.

Additional horizon solutions may be real and the result of different (possibly more generic) collapse histories; or just an artifact of our definition which does not single out the correct universal horizon. Since the spherical universal horizon in Schwarzschild case is suspected to become singular (26) by aspherical perturbations, the outermost universal horizon (that we have found) can potentially shield this singularity and save cosmic censorship. This further motivates numerical dynamical studies of *non-spherical* collapse in Lorentz-violating gravitational theories.

Gravitational dynamics within real black holes may yet have more surprises in store for us!

Chapter 2

Higher Dimensional Charged Randall Sundrum Black Holes.

2.1 Introduction

In (8) Randall and Sundrum proposed a novel approach to add extra unexperienced dimension for use in quantum gravity by considering a $4+1$ dimensional world where non-gravitational physics is constrained to a $3+1$ hypersurface (or brane), while gravitational effects are allowed to propagate through a bulk 5 dimensional AdS spacetime. At low energies, the theory reduces to 4D general relativity at distances large compared with the AdS length ℓ.

One is interested to find localized black hole solutions to find whether RS model is capable of recovering strong field predictions of general relativity for bulk dimension $N > 4$ (36). While a considerable amount of numerical work suggests such solutions exist (at least for small black holes) (37), there is still no analytic solution, except in $(2+1)$ dimensions (11). However it is known that there are no black hole solutions to General Relativity in $(2+1)$ dimension spacetime, leading to the conclusion that the existence of this solution is due to quantum corrections from the dual Conformal Field Theory. These corrections turn what would be a conical singularity classically into a regular horizon (38). While inducing a negative cosmological constant on the brane yields braneworld black hole solutions that are similar to those of $(2+1)$ dimensional AdS general relativity (39), large black holes are not localized on the brane.

In an attempt to make progress on this issue, Kaus and Reall (KR) (10), considered an extreme black hole charged with respect to an electromagnetic field on the brane. By examining the extremal solution KR can take advantage of symmetries of the near horizon geometry in the bulk solution . This approach has the bulk equations reduce to ordinary differential equations that integrate

to yield a 1-parameter family of solutions. Solving the Israel junction conditions to obtain the gravitational effect on the brane yields a relationship between this parameter and the charge on the brane, which then serves to label this family of solutions.

In this chapter, we seek to find extremal black hole solutions in $N = (n+1)$ bulk dimensions that contains an electromagnetic field on an n-dimensional brane. We seek to determine whether the structure exhibited by the $(4+1)$ dimensional extremal black hole is unique to that dimension of the brane and whether pathologies exist in higher dimensional braneworld theories. We do this by considering a sphere of dimension D (as opposed to 2 in KR) and solve the resulting field equations. By solving the Israel junction conditions on the brane we are able to determine the gravitational affect of the brane on the overall geometry. For $D = 2$ the structure of the Israel junction conditions determine the specific geometry of the spacetime, $k = -1$ (10). These arguments can then be continued to higher dimensions to again restrict to branes of the form $AdS^2 \times S^D$.

The work will first use an ansatz to find equations of motions that can be solved with a single parameter family of solutions. The electromagnetically charged brane will then be used to put junctions conditions on to which of those solutions are permissible. We will then look at the possible solutions in greater depth and delve into uncovering the structural relations between the charge and radius of the black hole. We see how the entropy measured in the brane and bulk differ and then construct an argument to find that for higher dimension than 5 the scaling of the entropy of small black holes is fundamentally different.

2.2 The Equations of Motion

The near horizon geometry of a static extreme black hole can be written in the warped product form (40)

$$ds^2 = A(z)^2(k)^2 d\Sigma^2 + dz^2 + R(z)^2 d\Omega_D^2 \tag{2.1}$$

with $d\Sigma^2 = -dt^2 + S(k)^2 dr^2$ where $S(0) = 1$, $S(-1) = \sin(t)$ and $S(1) = \sinh(t)$. Both t and r have been made unit less by using either ℓ the (A)dS radius for $k = \pm 1$ or some arbitrary length scale for $k = 0$. The co-ordinate z is the co-ordinate that moves us through the bulk, and $d\Omega_D^2$ is the line element on S^D, with $N-1 = D+2$ the dimension of the brane, and $N = D+3$ the overall dimension of the bulk.

The corresponding bulk Einstein field equations are given by

$$R_{\mu\nu} = -\frac{(D+2)}{\ell^2} g_{\mu\nu} \tag{2.2}$$

and inserting the black hole ansatz (2.1) into the field equations yields

$$\begin{aligned} \frac{k}{A^2}-\frac{A'^2}{A^2}-\frac{DA'R'}{AR}-\frac{A''}{A}&=-\frac{(D+2)}{\ell^2}\\ \frac{2A''}{A}+\frac{DR''}{R}&=\frac{(D+2)}{\ell^2}\\ \frac{(D-1)}{R^2}-\frac{(D-1)R'^2}{R^2}-\frac{2A'R'}{AR}-\frac{R''}{R}&=-\frac{(D+2)}{\ell^2}\end{aligned} \tag{2.3}$$

which reduce to the 5-dimensional version of (10) with $D = 2$. By denoting $R = \ell\,\rho(z/\ell)$ and $A = \ell\,\alpha(\rho/\ell)$ we can re-write the equations above as

$$\begin{aligned} \frac{k-\alpha'^2}{\alpha^2}-\frac{D\alpha'\rho'}{\alpha\rho}-\frac{\alpha''}{\alpha}&=-(D+2)\\ \frac{2\alpha''}{\alpha}+\frac{D\rho''}{\rho}&=(D+2)\\ \frac{(D-1)(1-\rho'^2)}{\rho^2}-\frac{2\alpha'\rho'}{\alpha\rho}-\frac{\rho''}{\rho}&=-(D+2)\end{aligned} \tag{2.4}$$

The Hamiltonian constraint is given by combining these three equations to eliminate the second order derivatives.

$$\frac{2(k-\alpha'^2)}{\alpha^2}-\frac{4D\alpha'\rho'}{\alpha\rho}+\frac{D(D-1)(1-\rho'^2)}{\rho^2}=-(D+2)(D+1) \tag{2.5}$$

Since the horizon is compact in the bulk, the D- sphere of the geometry must contract to a point. As a result $\rho(z/l)$ must vanish somewhere; this location can be chosen to be $z = 0$ without loss of generality. Requiring that the equations of motions are smooth at $z = 0$ then implies that.

$$\begin{aligned}\alpha(z/\ell)&=\sqrt{\frac{\beta}{D+2}}+\frac{\beta+k}{D+1}\left(\frac{D+2}{\beta}\right)^{1/2}\left(\frac{z}{\ell}\right)^2\\ &+\frac{\beta+k}{D+1}\left(\frac{(D-1)\beta-(3D+5)k}{(D+1)(D+3)}\right)\left(\frac{D+2}{\beta}\right)^{3/2}\left(\frac{z}{\ell}\right)^4\dots\end{aligned} \tag{2.6}$$

$$\begin{aligned}\rho(z/\ell)&=\frac{z}{\ell}+\frac{(D-1)\beta-2k}{D(D+1)}\left(\frac{D+2}{\beta}\right)\left(\frac{z}{\ell}\right)^3\\ &+\frac{\left(D^3+D^2+19D+3\right)\beta^2+4\left(5D^2+16D+3\right)k\beta+4\left(6D^2+13D+3\right)k^2}{D^2(D+1)^2(D+3)}\left(\frac{D+2}{\beta}\right)^2\left(\frac{z}{\ell}\right)^5\dots\end{aligned} \tag{2.7}$$

where $\alpha(0)=\sqrt{\frac{\beta}{D+2}}$ for some positive β

2.3 Junction Conditions

The $n = N - 1$ dimensional brane action is given by

$$S_{\text{brane}}=\int d^nz\sqrt{-h}\left(-\sigma-\frac{1}{16\pi G_n}F_{ij}F^{ij}\right) \tag{2.8}$$

where h_{ij} is the induced metric on the brane, σ is the brane tension, G_n is Newton's constant on the brane, and F is the electromagnetic field on the brane. The tension of the brane is given by $\sigma = (N-2)/4\pi G_N \ell$ and $G_n = (N-3)G_N/2\ell$(39). The action results in an energy-momentum tensor of

$$T_{ab} = \frac{1}{4\pi G_n} F_{ai} F_b{}^i - h_{ab}\left(\sigma + \frac{1}{16\pi G_n} F_{ij}F^{ij}\right)$$

$$T = -\frac{N-5}{16\pi G_n} F_{ij}F^{ij} - (N-1)\sigma$$

Thus from Israel junction conditions (32) as derived in the appendix and assuming that the brane located at $z = z_0$ is $\mathbb{Z}_2$ symmetric about z_0 and thus $K_{ab}(z_0^+) = -K_{ab}(z_0^-)$ we find

$$\begin{aligned} K_{ab}(z_0) &= \frac{8\pi G_N}{2}\left(\frac{1}{N-2}\left(-\frac{N-5}{16\pi G_n}F_{ij}F^{ij} - (N-1)\sigma\right)h_{ab} + \frac{-1}{4\pi G_n}F_{ai}F_b{}^i \right. \\ &\quad \left. + h_{ab}\left(\sigma + \frac{1}{16\pi G_n}F_{ij}F^{ij}\right)\right) \\ &= \frac{-4\pi G_N \sigma}{N-2}h_{ab} + \frac{G_N}{G_n}\left(\frac{3}{4(N-2)}h_{ab}F_{ij}F^{ij} - F_{ai}F_b{}^i\right) \\ &= \frac{-1}{\ell}h_{ab} + \frac{2\ell}{N-3}\left(\frac{3}{4(N-2)}F_{ij}F^{ij}h_{ab} - F_{ai}F_b{}^i\right) \end{aligned} \tag{2.9}$$

which up to a sign convention reduces down to the $N = 5$ case of (10). We assume the electromagnetic field to be spherically symmetric and purely electric, yielding

$$\star_n F = Q_D \mathrm{d}\Omega_D \tag{2.10}$$

where $\star_n$ is the Hodge dual in n dimensions, F is the Faraday differential form, and $d\Omega_D$ is the volume form on a D sphere. Given that for a $2-$form on a Lorentzian manifold ω the Hodge dual satisfies $\star_n \star_n \omega = -\omega$ one finds that the electromagnetic field strength is given by

$$F = -\star_n \star_n F = -Q_D \star_n (\mathrm{d}\Omega_D) = -Q_D \frac{S(k)A(z_0)^2}{R(z_0)^D}\mathrm{d}t \wedge \mathrm{d}r \tag{2.11}$$

We can use the definition of extrinsic curvature on our chosen metric and normal vector to write $K_{ab} = \frac{-1}{2}\partial_z(g_{ab})\big|_{z=z_0}$. Thus the junction conditions (2.9) can be simplified to

$$\begin{aligned} \frac{-1}{2}\partial_z(g_{ab})\bigg|_{z=z_0} &= \frac{-1}{\ell}h_{ab} + \frac{2\ell}{N-3}\left(\frac{3}{4(N-2)}\frac{-2Q_D^2}{R(z_0)^{2D}}h_{ab} - \frac{Q_D^2 A(z_0)^2}{R(z_0)^{2D}}\left(\delta_a^t\delta_b^t - S(k)^2\delta_a^r\delta_b^r\right)\right) \\ \implies \frac{1}{2}\partial_z(g_{ab})\bigg|_{z=z_0} &= \frac{1}{\ell}h_{ab} + \frac{2\ell}{N-3}\left(\frac{3}{2(N-2)}\frac{Q_D^2}{R(z_0)^{2D}}h_{ab} + \frac{Q_D^2 A(z_0)^2}{R(z_0)^{2D}}\left(\delta_a^t\delta_b^t - S(k)^2\delta_a^r\delta_b^r\right)\right) \end{aligned} \tag{2.12}$$

These equations create two independent constraints which after some rearrangement become

$$\frac{A'(z_0)}{A(z_0)} = \frac{1}{\ell} - \frac{2N-7}{(N-3)(N-2)}\frac{\ell Q_D^2}{R(z_0)^{2D}} \qquad \frac{R'(z_0)}{R(z_0)} = \frac{1}{\ell} + \frac{3}{(N-3)(N-2)}\frac{\ell Q_D^2}{R(z_0)^{2D}}. \tag{2.13}$$

These can be rewritten in term of the α and ρ defined above as

$$\frac{\alpha'(z_0/\ell)}{\alpha(z_0/\ell)} = 1 - \frac{2N-7}{(N-3)(N-2)}\frac{q_D^2}{\rho(z_0/\ell)^{2D}} \qquad \frac{\rho'(z_0/\ell)}{\rho(z_0/\ell)} = 1 + \frac{3}{(N-3)(N-2)}\frac{q_D^2}{\rho(z_0/\ell)^{2D}}. \tag{2.14}$$

where $q_D = Q/\ell^{D-1}$. These conditions can be combined and rearranged to where we can obtain the following conditions

$$3\frac{\alpha'(z_0/\ell)}{\alpha(z_0/\ell)} + (2D-1)\frac{\rho'(z_0/\ell)}{\rho(z_0/\ell)} = 2(D+1) \qquad q_D = \rho(z_0)^D\sqrt{\frac{D}{2}\left(\frac{\rho'(z_0)}{\rho(z_0)} - \frac{\alpha'(z_0)}{\alpha(z_0)}\right)} \tag{2.15}$$

The Hamiltonian constraint can also be evaluated at $z = z_0$ to give

$$\frac{7D-2}{d^2(d+1)}\frac{q^4}{\rho(z_0/\ell)^{4D}} + \frac{2(D-2)}{D}\frac{q^2}{\rho(z_0/\ell)^{2D}} + \frac{D(D-1)}{\rho(z_0/\ell)^2} = \frac{-2k}{\alpha(z_0/\ell)^2} \tag{2.16}$$

and as each term on the right hand side is positive individually we find that $k = -1$, eliminating the other choices.

2.4 Solutions

We can now restrict ourselves to $k = -1$ which affords us two exact solutions. We will first look at the properties of the two exact solutions and then explore the remainder of the parameter space.

The two analytic solutions are a generalization of those found in (10). For the first case sets $\beta = D + 2$ or $\alpha(0) = 1$ and results are

$$\alpha(z/\ell) = \cosh(z/\ell)) \qquad \rho(z/\ell) = \sinh(z/\ell) \tag{2.17}$$

However this would require $z_0/\ell = \operatorname{arctanh}\left(\frac{1}{3}(2d-1)\right)$ or $z_0/\ell = \operatorname{arctanh}(1) = \infty$ neither of which are real for $d \geq 2$. Some may find interest in the $z = \infty$ solution, but the meaning of the junction conditions becomes unclear here. If one could make sense of these conditions in this limit a re-examination of $k = 0, 1$ may be in order. The numerically observed behaviour of α and ρ for these values of k both tend towards being proportional $e^{z/\ell}$ for the large z limit leading to (2.15) and (2.16) holding.

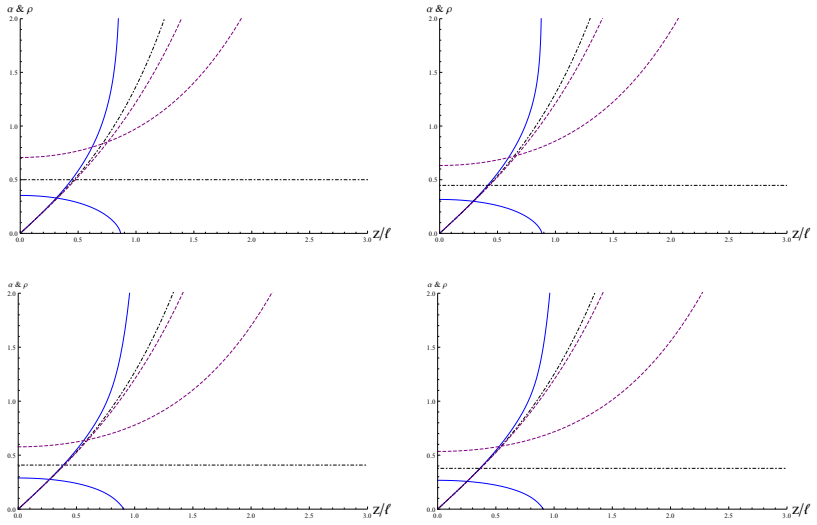

Figure 2.1: Plots of the behaviour of $\rho(z/\ell)$ (curves starting at 0) and $\alpha(z/\ell)$ (curve starting at finite value). D runs from 2 to 5 running across first then down. β takes the values of $1/2$ (solid blue), 1 (Dot-Dashed black) and 2 (Dashed Purple).

The second exact solution sets $\beta = 1$ which results in α being constant

$$\alpha(z/\ell) = \frac{1}{\sqrt{D+2}} \qquad \rho(z/\ell) = \sqrt{\frac{D}{D+2}} \sinh\left(\sqrt{\frac{D+2}{D}}\frac{z}{\ell}\right). \tag{2.18}$$

Using the Israel junction conditions, we find that we can express q_D, ρ_0 exactly as

$$z_0 = \sqrt{\frac{D}{D+2}} \operatorname{arccoth}\left(\frac{2D+2}{2D-1}\sqrt{\frac{D}{D+2}}\right) \tag{2.19}$$

$$q_D = \sqrt{\frac{2D+2}{2D-1}}\left((2D-1)\sqrt{\frac{D}{4D^2+11D-2}}\right)^D \tag{2.20}$$

For general values of β, we will rely on numeric techniques. As our equations of motion are singular at 0, we must rely on the expansions (2.6) and (2.7) taken to $\mathcal{O}(\left(\frac{z}{\ell}\right)^{22})$ which can be evaluated at $z = 10^{-16}\ell$ to generate initial conditions. In general, we find two kinds of behaviour surrounding the case of constant α which can be seen in figures (2.1). For $\beta > 1 \implies \alpha(0) > \sqrt{1/(D+2)}$ we find that α and ρ tend towards being proportional to $e^{z/\ell}$ for large z, see figure (2.2). While for $\beta < 1$ we see new behaviour where α monotonically decreases to 0, for some finite z_1, at which point ρ also diverges. A calculation of the

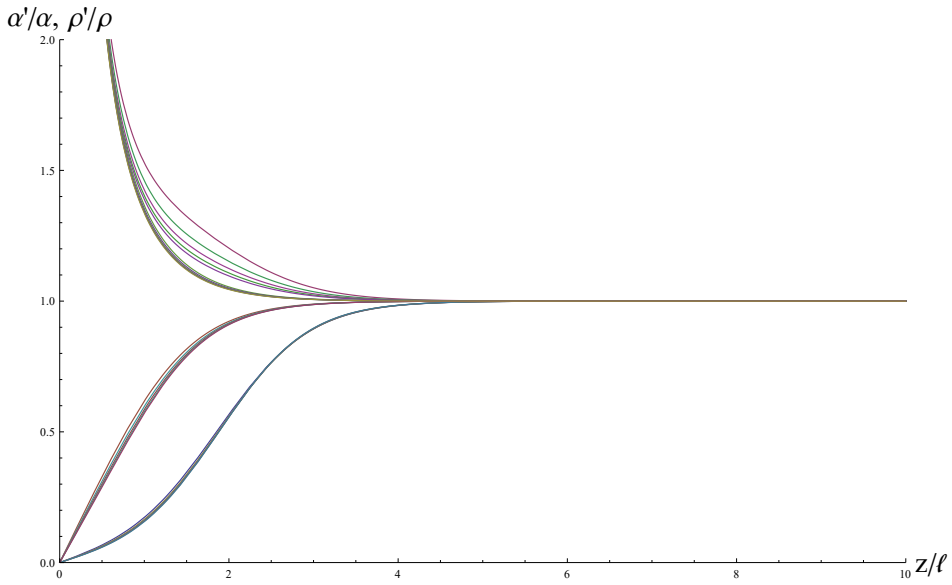

Figure 2.2: ρ'/ρ (upper curves) and α'/α (lower curves) of $\beta = 1.1, 2$ for $D = 2, 3, 4, 5, 6$. This behaviour persists for all $\beta > 1$ tested. We conclude $\alpha(z/\ell), \rho(z/\ell) \propto e^{z/\ell}$. For constant β lines move left as D increases. Holding D constant while increasing β also causes curves to tend to the left.

Kretschmann scalar indicates that there is a curvature singularity at z_1. This singularity would be naked if the brane , and therefore the $\mathbb{Z}_2$ flip across it was not placed before it. In all our simulations we find $z_0 < z_1$ meaning the area of the solution is not reached in the full RS model.

While the equations of motions always have solutions, the junctions conditions eliminate more of the parameter space. When $D = 2$ in (10), they found that the limiting case was the first analytic solutions described above. For all $\alpha(0) < 1$, solutions were found, however for $D > 2$ this is no longer the case. We find that the value of the upper bound of $\alpha(0)$ is not easily characterized. In figure (2.3) we plot z_0/ℓ for various values of $\alpha(0)$ and we can see that z_0 seems to diverge for some value of $\alpha(0)$ which decreases with D, see table (2.1) for the value of the bounding $\alpha(0)$. Below this bound, we find that solutions exist for all positive $\alpha(0)$ with $z_0 \propto \alpha(0)$ for small initial values.

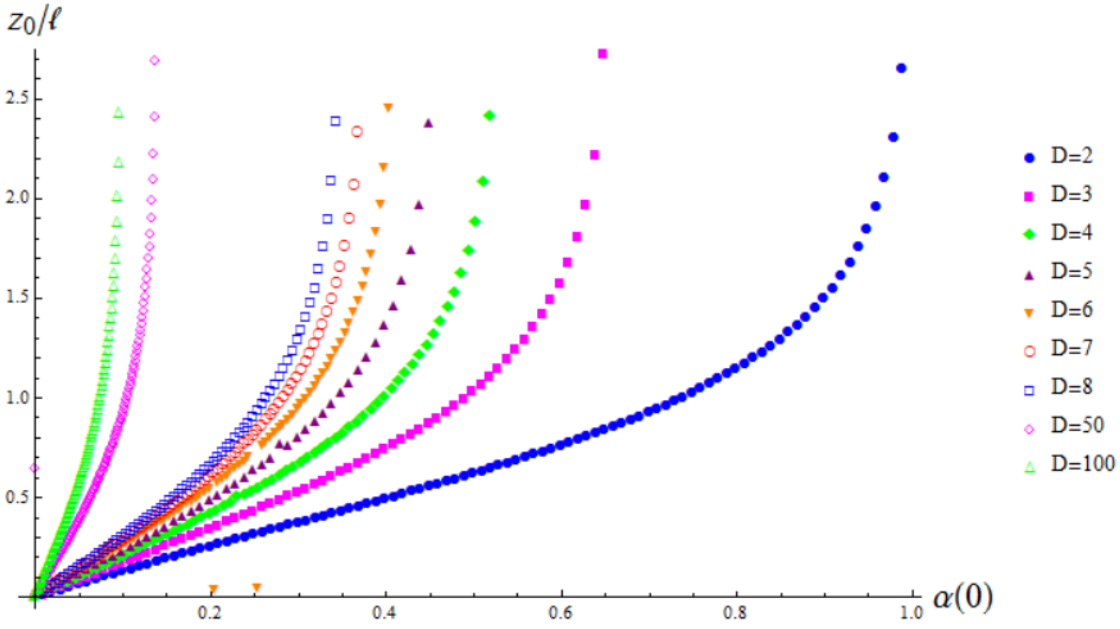

Figure 2.3: The location of the brane z_0/ℓ of differing initial radii of the AdS_2 space for various spherical dimensions.

Spherical Dimension ($D = N - 3$)	Bounding $\alpha(0)$
2	1
3	≈ 0.66
4	≈ 0.53
5	≈ 0.46
6	≈ 0.42
7	≈ 0.38
8	≈ 0.35
50	≈ 0.14
100	≈ 0.10

Table 2.1: The bounding value of $\alpha(0)$ of higher bulk dimension

We now switch to a parametrisation in terms of the more physically natural parameter of charge, q_D to find the behaviour of $\alpha(z_0), \rho(z_0)$ for large z_0. We can use the scaling of q_D with ℓ to guess that

$$\alpha(z_0) = \gamma_{(\alpha,D)} q_D^{1/D-1} \qquad \rho(z_0) = \gamma_{(\rho,D)} q_D^{1/D-1} \qquad \text{for } q_D >> 1 \tag{2.21}$$

where $\gamma_{(\alpha,D)}$ and $\gamma_{(\rho,D)}$ are constants dependant on dimension. Figures (2.4) demonstrate this behaviour for the first few dimensions and figure (2.5) shows the behaviour of the numerically found constants. We note that for extremely small q_D both $\alpha(z_0)/q^{1/(D-1)}$ and $\rho(z_0)/q^{1/(D-1)}$ diverge, but the scale is incredibly small.

2.5 Entropy of Large Black Holes

The Bekenstein-Hawking entropy of the black hole is given as

$$S_{D+3} = \frac{2\pi}{G_{D+3}} \int_0^{z_0} dz\, R(z)^D = \frac{2\pi \ell^D}{G_{D+3}} \int_0^{z_0} dz\, \rho(z/\ell)^D$$

When $z_0 \gg \ell$, we find ρ is dominated by the term near $z = z_0$ and thus Figure (2.2) suggest that it is safe to treat $\rho(z/\ell) \approx \rho(z_0/\ell) e^{(z-z_0)/l}$. Thus the bulk entropy is

$$S_{D+3} \approx \frac{2\pi \ell^D}{G_{D+3}} \rho(z_0/\ell)^D e^{-Dz_0/\ell} \int_0^{z_0} dz\, e^{Dz/\ell} \approx \frac{2\pi \ell^{D+1}}{D G_{D+3}} \rho(z_0/\ell)^D \quad \text{for large } z_0.$$

Recalling that $\rho(z_0/\ell) = \gamma_{(\rho,D)} q_D^{1/(D-1)}$, $q_D = Q_D/\ell^{D-1}$ and $G_{D+2} = DG_{D+3}/\ell$ we can simplify this to

$$S_{D+3} \approx \frac{2\pi \ell^{D+1}}{D G_{D+3}} \gamma^D_{(\rho,D)} q_D^{D/(D-1)} = \frac{2\pi \ell}{D G_{D+3}} \gamma^D_{(\rho,D)} Q_D^{D/(D-1)} = \frac{\pi}{G_{D+2}} \gamma^D_{(\rho,D)} Q_D^{D/(D-1)} \quad \text{for large } z_0.$$

We can then compare this to the n-dimensional entropy expected on the brane

$$S_{D+2} = \frac{\pi^{(D+1)/2}}{2G_{D+2}\Gamma((D+1)/2)} Q_D^{D/(D-1)}$$

Thus we find

$$\frac{S_{D+3}}{S_{D+2}} = \frac{2\Gamma((D+1)/2)}{\pi^{(D-1)/2}} \gamma^D_{(\rho,D)} = \frac{4\pi}{\mathcal{A}_{D+1}} \gamma^D_{(\rho,D)} \quad \text{for large } z_0,$$

where $\mathcal{A}_{D+1}$ is the coefficient describing surface area of a unit $(D+1)$sphere. It is interesting to note that for large D, the surface area of a unit sphere vanishes quickly with D meaning that unless $\gamma^D_{(\rho,D)}$ shrank faster, the ratio between the two entropies diverges. However, as can be seen 2.5 $\gamma_{(\rho,D)}$ seems to recover after its minimum at $D = 4$, in fact we numerically find that ($\gamma_{(\rho,D)} \to 1$ for large D.

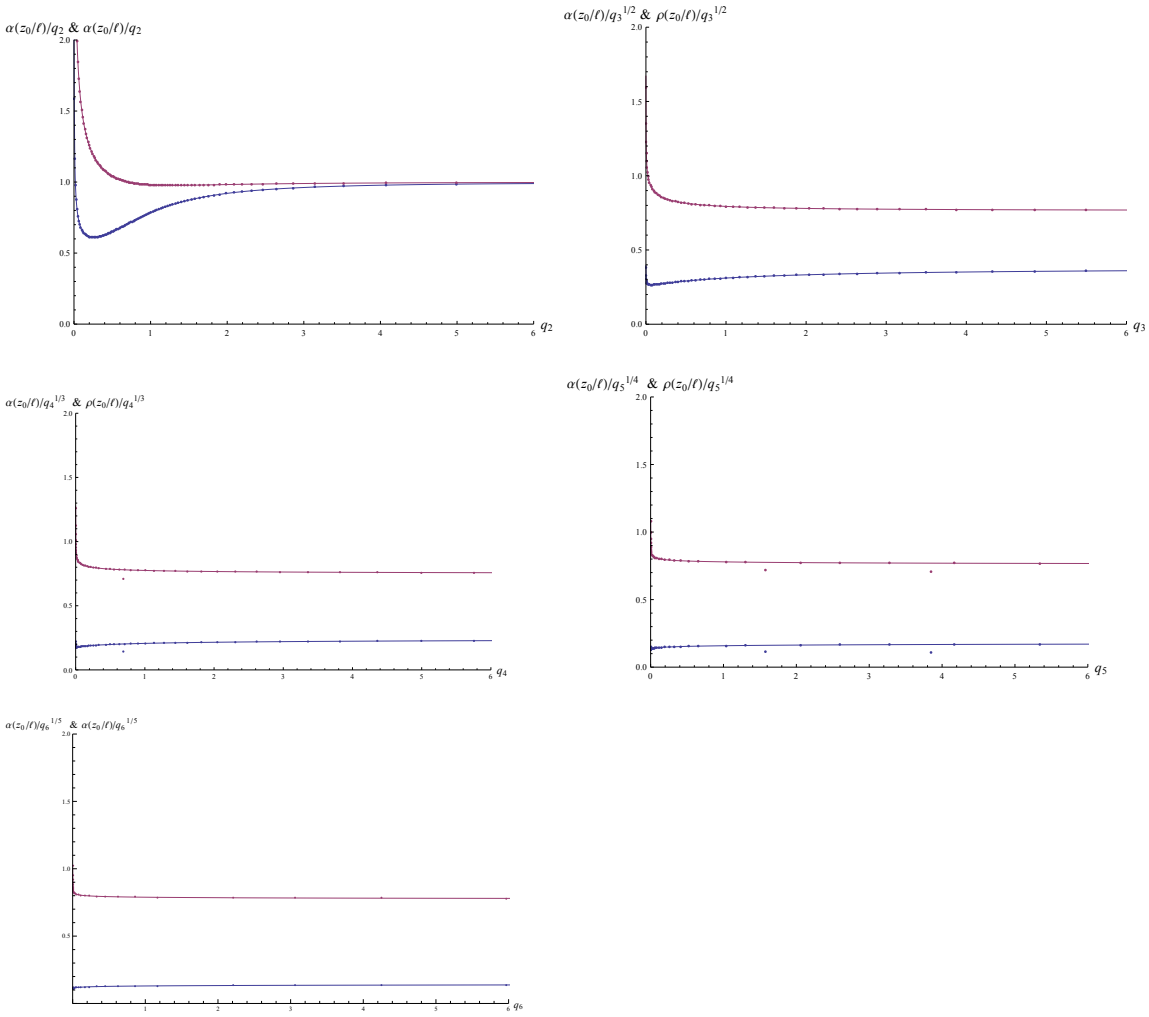

Figure 2.4: The ratios between $\alpha(z_0/\ell)$ (lower blue curves) and $\rho(z_0/\ell)$ (upper magenta curves) to $q_D^{1/(D-1)}$. The dimension of the hypersphere D run from 2 to 6 starting in the top left then proceeding across and then down. It is worth noting that only in the already studied $D = 2$ case both ratios converge to unity. In all others the ratios differs from unity. The converged ratio is denoted $\gamma_{(\alpha,D)}$ and $\gamma_{(\rho,D)}$ respectively

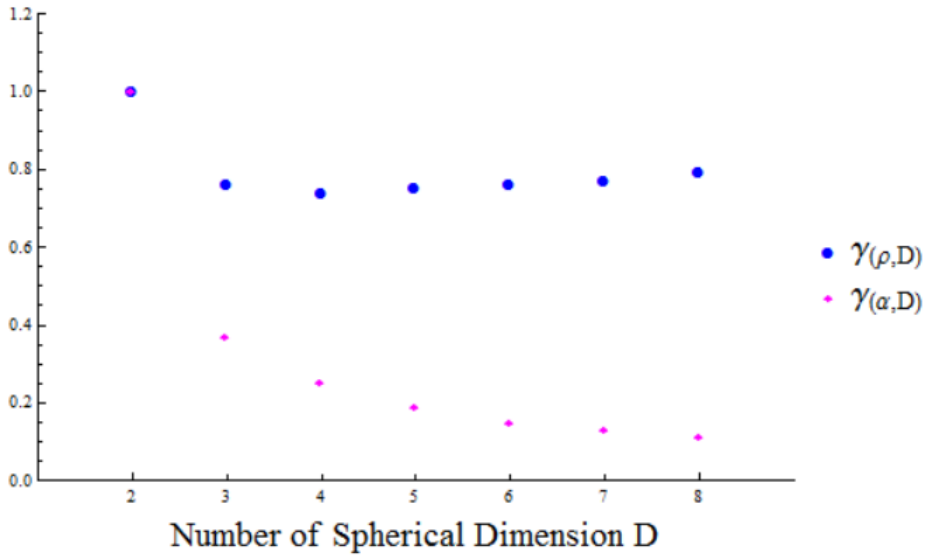

Figure 2.5: Numerically found ratio between $\alpha(z_0/\ell)$ and $\rho(z_0/\ell)$ and $q_D^{1/(D-1)}$ for large q_D

2.6 Entropy of Small black holes

Figure (2.3) suggest that for small z_0, $z_0 \propto \alpha(0)$. As such by their expansions (2.6) and (2.7) to first order $\alpha(z_0)$ and $\rho(z_0)$ all scale as $\alpha(0)$. From the second relation of (2.15), we find that $\rho(z_0) \propto q_D^{2/(2D-1)}$ in the regime of small z_0 where $\rho'(z_0) \approx 1$ and $\alpha'(z_0) = 0$. Consequently, by transitivity $z_0, \alpha(z_0), \alpha(0) \propto q_D^{2/(2D-1)}$. Thus $\alpha(z_0)/q_D^{1/(D-1)} \propto q_D^{-1/(2D-1)(D-1)}$ which demonstrates the divergence of that ratio for $q_D \to 0$. The identical scaling applies to $\rho(z_0)$ and accounts for the similar behaviour of its ratio for small q_D. We then find

$$S_{D+3} \propto \int_0^{z_0} \mathrm{d}z \rho^D(z/\ell) \approx \frac{\ell}{D+1}\rho(0)^{D+1} \propto \ell q_D^{2(D+1)/(2D-1)}$$

Unlike the specific case of $D = 2$, general D do not satisfy $\frac{D}{D-1} \neq \frac{2(D+1)}{2D-1}$ and as a result we find that our entropy scaling changes at the scale of small z_0.

2.7 Discussion

In this chapter, we looked for extremally charged black hole solutions for a higher dimensional Randall Sundrum model. We found, much like the work of (10) for $N = 5$, that, while the equations of motion for the near horizon geometry allow for the space to have a subspace which is any 2D Lorentzian manifold, only the choice of AdS_2 allow for satisfaction of the junction conditions.

When looking to compare with the expected observations of entropy for the black holes of a standard GR model, we find that black holes which are large compared to the AdS radius retain an identical scaling dependence. There is also an argument made for small black holes that expected scaling is not maintained. This discrepancy leaves room for inquiry of how these new scaling relations affect the geometry in a dynamical system.

This change in entropy scaling may be expected as the RS model can only recover perturbative Newtonian gravity when at scales that are large compared to ℓ. In KR's work it may just be a coincidence that there is matching when they begin to look at smaller black holes.

Furthermore, if work could be done to overcome the challenges of non-static systems, questions could arise as to whether the numerically found coefficients for entropy are dimensionally dependent or if they are a feature of each specific spacetime.

Bibliography

[1] M. Meiers, M. Saravani, and N. Afshordi, "Cosmic Censorship in Lorentz Violating Theories of Gravity," *Phys. Rev.*, vol. D93, p. 104008, 2016.

[2] I. Zlatev, L. Wang, and P. J. Steinhardt, "Quintessence, Cosmic Coincidence, and the Cosmological Constant,", *arxiv:astro-ph/9807002v2*

[3] P. Steinhardt, *Critical Problems in Physics*. Princeton U. Press, 1997.

[4] E. Babichev, V. Mukhanov, and A. Vikman, "k-Essence, superluminal propagation, causality and emergent geometry," *JHEP*, vol. 02, p. 101, 2008.

[5] N. Afshordi, D. Chung, and G. Geshnizjani, "Cuscuton: A Causal Field Theory with an Infinite Speed of Sound," *Phys. Rev.*, vol. D75, p. 75.083513, 2006.

[6] N. Afshordi, "Cuscuton and low energy limit of Horava-Lifshitz gravity," *Phys. Rev.*, vol. D80, p. 081502, 2009.

[7] M. Saravani, N. Afshordi, and R. Mann, "Dynamical Emergence of Universal Horizons during the formation of Black Holes," *Phys. Rev.*, vol. D89, p. 084029, 2014.

[8] L. Randall and R. Sundrum., "An alternative to compactification," *Phys. Rev. Lett.*, vol. 83, pp. 1663–1666, 1999.

[9] P. Figueras and T. Wiseman, "Gravity and Large Black Holes in Randall-Sundrum II Braneworlds," *Phys. Rev. Lett.*, vol. 107, p. 081101, 2011.

[10] A. Kaus and H. Reall, "Charged Randall-Sundrum black holes and $\mathcal{N} = 4$ super Yang-Mills in $AdS_2 \times S^2$," 2009.

[11] G. T. H. R. Emparan and R. C. Myers, "Exact description of black holes on branes," *JHEP*, vol. 007, 2000.

[12] D. G. Boulware and S. Deser, "Can gravitation have a finite range?," *Phys. Rev.*, vol. D6, pp. 3368–3382, 1972.

[13] K. S. Stelle, "Renormalization of Higher Derivative Quantum Gravity," *Phys. Rev.*, vol. D16, pp. 953–969, 1977.

[14] P. Horava, "Quantum Gravity at a Lifshitz Point," *Phys. Rev.*, vol. D79, p. 084008, 2009.

[15] N. Afshordi, "Why is High Energy Physics Lorentz Invariant?,", *arXiv:hep-th/1511.07879*

[16] D. Blas, O. Pujolas, and S. Sibiryakov, "Models of non-relativistic quantum gravity: The Good, the bad and the healthy," *JHEP*, vol. 04, p. 018, 2011.

[17] T. Jacobson and D. Mattingly, "Gravity with a dynamical preferred frame," *Phys. Rev.*, vol. D64, p. 024028, 2001.

[18] T. Jacobson, "Lorentz violation and Hawking radiation," in *CPT and Lorentz symmetry. Proceedings: 2nd Meeting, Bloomington, USA, Aug 15-18, 2001*, pp. 316–320, 2002.

[19] T. P. Sotiriou, I. Vega, and D. Vernieri, "Rotating black holes in three-dimensional Ho?ava gravity," *Phys. Rev.*, vol. D90, no. 4, p. 044046, 2014.

[20] C. Ding, A. Wang, and X. Wang, "Charged Einstein-aether black holes and Smarr formula,", *arXiv:gr-qc/1507.06618*

[21] E. Barausse and T. P. Sotiriou, "Slowly rotating black holes in Horava-Lifshitz gravity," *Phys. Rev.*, vol. D87, p. 087504, 2013.

[22] J. Bhattacharyya, M. Colombo, and T. P. Sotiriou, "Causality and black holes in spacetimes with a preferred foliation,", *arXiv:gr-qc/1509.01558*

[23] E. Barausse and T. P. Sotiriou, "Black holes in Lorentz-violating gravity theories," *Class. Quant. Grav.*, vol. 30, p. 244010, 2013.

[24] E. Babichev, V. F. Mukhanov, and A. Vikman, "Escaping from the black hole?," *JHEP*, vol. 09, p. 061, 2006.

[25] E. Barausse, T. Jacobson, and T. P. Sotiriou, "Black holes in Einstein-aether and Horava-Lifshitz gravity," *Phys. Rev.*, vol. D83, p. 124043, 2011.

[26] D. Blas and S. Sibiryakov, "Horava gravity versus thermodynamics: The Black hole case," *Phys. Rev.*, vol. D84, p. 124043, 2011.

[27] A. Mohd, "On the thermodynamics of universal horizons in Einstein-Æther theory," 2013.

[28] P. Berglund, J. Bhattacharyya, and D. Mattingly, "Mechanics of universal horizons," *Phys. Rev.*, vol. D85, p. 124019, 2012.

[29] P. Berglund, J. Bhattacharyya, and D. Mattingly, "Towards Thermodynamics of Universal Horizons in Einstein-ther Theory," *Phys. Rev. Lett.*, vol. 110, no. 7, p. 071301, 2013.

[30] J. Bhattacharyya and D. Mattingly, "Universal horizons in maximally symmetric spaces," *Int. J. Mod. Phys.*, vol. D23, no. 13, p. 1443005, 2014.

[31] F. Michel and R. Parentani, "Black hole radiation in the presence of a universal horizon," *Phys. Rev.*, vol. D91, no. 12, p. 124049, 2015.

[32] K. Maeda, "Gravitational Collapse of Charged Dust Shell and Maximal Slicing Condition," *Progress of Theoretical Physics*, vol. 63, no. 2, pp. 425–437, 1980.

[33] W. Israel and V. de la Cruz, "Gravitational bounce," *Il Nuovo Cimento A Series 10*, vol. 51, pp. 744–760, 1967.

[34] E. Poisson and W. Israel, "Inner-horizon instability and mass inflation in black holes," *Phys. Rev. Lett.*, vol. 63, pp. 1663–1666, 1989.

[35] E. Barausse, T. P. Sotiriou, and I. Vega, "Slowly rotating black holes in Einstein-æther theory," 2015.

[36] R. Gregory, "Braneworld black holes,", *arXiv:hep-th/0804.2595v1*

[37] T. T. H. Kudoh and T. Nakamura, "Small localized black holes in braneworld:Formulation and numerical method," *Phys. Rev. D*, vol. 68, 2003.

[38] A. F. R. Emparan and N. Kaloper, "Exact description of black holes on branes," *JHEP*, vol. 043, 2000.

[39] G. T. H. R. Emparan and R. C. Myers, "Exact description of black holes on JHEP, vol. 021, 2000.

[40] J. L. H. K. Kunduri and H. Reall, "Near-horizon symmetries of extremal black holes," *Class. Quant. Grav.*, vol. 24, 2007.

Appendix

Junction Condition

We generalize the Junction conditions made for N=5 bulk in (36) to bulks of arbitrary dimension. We make use of Israel's technique and break up our N dimensional bulk into a family of $N-1$ dimensional sub-manifolds described by the coordinates x^a, and a normal distance from a particular surface z. To distinguish between tensors which lie in the full space or only on the hypersurfaces, we will use Greek for the former and Latin for the latter. Let the metric in the bulk take the form

$$\mathrm{d}s^2 = h_{ab}(x,z)\mathrm{d}x^a\mathrm{d}x^b + \mathrm{d}z^2$$

where h_{ab} lies in the tangent space of the sub-manifolds which encapsulates the information in the intrinsic metric. We can also bring h into the full space to act as a projection metric to find the surface parallel components of tensors in the tangent space of the bulk. To bring h up, let us define $n^\mu = \delta^\mu_z$ which describes the direction normal to each surface. The projection tensor thus takes the form

$$\tilde{h}_{\mu\nu} = g_{\mu\nu} - n_\mu n_\nu$$

We will use the tilde to bring an element of the tangent space of the $N-1$ dimensional structure into the tangent space of the N dimensional space via an inclusion map. The data encoded in h could be employed to find the intrinsic curvature on the surface, but we have more interest in connecting the bulk's curvature to the h. In order to do this connection, we need a means to measure the bending of the surface in the larger space. This bending is measured using the extrinsic curvature

$$K_{\mu\nu} = \tilde{h}^\alpha_\mu \tilde{h}^\beta_\nu \nabla_\alpha n_\beta$$

which clearly is tangential to the hypersurface, and although subtle in this form, it can be shown to be symmetric. There are a few results which also follow from our choice of the Gauss Normal gauge. The first uses that $n_\mu n^\mu = 1$ for all coordinates which implies that $0 = \frac{1}{2}\nabla_\alpha(n_\mu n^\mu) = n^\mu \nabla_\alpha(n_\mu)$. Consequentially,

$$K_{\mu\nu} = \tilde{h}^\alpha_\mu \tilde{h}^\beta_\nu \nabla_\alpha n_\beta = \tilde{h}^\alpha_\mu(\delta^\beta_\nu - n^\beta n_\nu)\nabla_\alpha n_\beta = \tilde{h}^\alpha_\mu(\nabla_\alpha n_\nu - n_\nu n^\beta \nabla_\alpha n_\beta) = \tilde{h}^\alpha_\mu \nabla_\alpha n_\nu. \tag{22}$$

which allows us to not need the second projection. In fact, because $n^\mu = \delta^\mu_z$ implying $\partial_\mu n^\nu = 0$ and $g_{z\mu} = \delta^z_\mu$ one can conclude

$$n^\mu \nabla_\mu n_\nu = n^\mu \left(\frac{1}{2}\partial_z g_{\mu\nu}\right) = \left(\frac{1}{2}\partial_z g_{z\nu}\right) = 0.$$

As a result of this property, we can further simplify the extrinsic curvature to require no projections

$$K_{\mu\nu} = \tilde{h}^\alpha_\mu \nabla_\alpha n_\nu = (\delta^\alpha_\mu - n_\mu n^\alpha)\nabla_\alpha n_\nu = \nabla_\mu n_\nu. \tag{23}$$

Finally, we make note of two identities

$$\nabla_\mu \tilde{h}^\beta_\alpha = -K_{\mu\alpha} n^\beta - K_\mu{}^\beta n_\alpha \tag{24}$$

which follow from (23) and the Leibniz rule, and another for the Lie derivative of the extrinsic curvature

$$\mathcal{L}_n K_{\mu\nu} = n^\lambda \nabla_\lambda K_{\mu\nu} + K_{\lambda\nu}\nabla_\mu n^\lambda + K_{\mu\lambda}\nabla_\nu n^\lambda = n^\lambda \nabla_\lambda K_{\mu\nu} + 2K_{\mu\lambda}K_\nu{}^\lambda. \tag{25}$$

With these tools outlined, we proceed to prove the Gauss-Codazzi relation. The derivation begins with the relation between the surfaces, Riemann tensor and the commutation of the tangential covariant derivative

$$\tilde{R}^{(N-1)\,\mu}{}_{\lambda\alpha\beta} v^\lambda = [\tilde{\nabla}_\alpha, \tilde{\nabla}_\beta] v^\mu.$$

where v lies in the tangent space of the hypersurface. The entire expression must be projected after each derivative to restrict the effect to what would be intrinsic to the surface. For clarity, we will look at the first term of commutation on its own first.

$$\begin{aligned}
\tilde{\nabla}_\alpha \tilde{\nabla}_\beta v^\mu &= \tilde{h}^{\alpha'}_\alpha \tilde{h}^{\beta'}_\beta \tilde{h}^\mu_{\mu'} \nabla_{\alpha'} \left(\tilde{h}^{\beta''}_{\beta'} \tilde{h}^{\mu'}_{\mu''} \nabla_{\beta''} \left(v^{\mu''}\right)\right) \\
&= \tilde{h}^{\alpha'}_\alpha \tilde{h}^{\beta'}_\beta \tilde{h}^\mu_{\mu'} \tilde{h}^{\mu'}_{\mu''} \nabla_{\beta''} \left(v^{\mu''}\right) \nabla_{\alpha'} \left(\tilde{h}^{\beta''}_{\beta'}\right) + \tilde{h}^{\alpha'}_\alpha \tilde{h}^{\beta'}_\beta \tilde{h}^\mu_{\mu'} \tilde{h}^{\beta''}_{\beta'} \nabla_{\beta''} \left(v^{\mu''}\right) \nabla_{\alpha'} \left(\tilde{h}^{\mu'}_{\mu''}\right) \\
&+ \tilde{h}^{\alpha'}_\alpha \tilde{h}^{\beta'}_\beta \tilde{h}^\mu_{\mu'} \tilde{h}^{\beta''}_{\beta'} \tilde{h}^{\mu'}_{\mu''} \nabla_{\alpha'} \nabla_{\beta''} v^{\mu''} \\
&= \tilde{h}^{\alpha'}_\alpha \tilde{h}^{\beta'}_\beta \tilde{h}^\mu_{\mu'} \nabla_{\beta''} \left(v^{\mu'}\right) \left(-K_{\alpha'\beta'} n^{\beta''} - K_{\alpha'}{}^{\beta''} n_{\beta'}\right) \\
&+ \tilde{h}^{\alpha'}_\alpha \tilde{h}^{\beta'}_\beta \tilde{h}^\mu_{\mu'} \nabla_{\beta'} \left(v^{\mu''}\right) \left(-K_{\alpha'\mu''} n^{\mu'} - K_{\alpha'}{}^{\mu'} n_{\mu''}\right) \\
&+ \tilde{h}^{\alpha'}_\alpha \tilde{h}^{\beta'}_\beta \tilde{h}^\mu_{\mu'} \nabla_{\alpha'} \nabla_{\beta'} v^{\mu'} \\
&= -K_{\alpha\beta} n^{\beta''} \tilde{h}^\mu_{\mu'} \nabla_{\beta''} v^{\mu'} - K_\alpha{}^\mu \tilde{h}^{\beta'}_\beta n_{\mu''} \nabla_{\beta'} v^{\mu''} + \tilde{h}^{\alpha'}_\alpha \tilde{h}^{\beta'}_\beta \tilde{h}^\mu_{\mu'} \nabla_{\alpha'} \nabla_{\beta'} v^{\mu'}
\end{aligned}$$

The first term is symmetric in α and β and will disappear in the commutation while the other two remain. Thus we have

$$\begin{aligned}
\tilde{R}^{(N-1)\,\mu}{}_{\lambda\alpha\beta} v^\lambda &= K_\beta{}^\mu \tilde{h}_\alpha^{\alpha'} n_{\mu''} \nabla_{\alpha'} v^{\mu''} - K_\alpha{}^\mu \tilde{h}_\beta^{\beta'} n_{\mu''} \nabla_{\beta'} v^{\mu''} + \tilde{h}_\alpha^{\alpha'} \tilde{h}_\beta^{\beta'} \tilde{h}_{\mu'}^{\mu} \left(\nabla_{\alpha'} \nabla_{\beta'} v^{\mu'} - \nabla_{\beta'} \nabla_{\alpha'} v^{\mu'} \right) \\
&= \left(K_\beta{}^\mu \tilde{h}_\alpha^\rho - K_\alpha{}^\mu \tilde{h}_\beta^\rho \right) n_\lambda \nabla_\rho v^\lambda + \tilde{h}_\alpha^{\alpha'} \tilde{h}_\beta^{\beta'} \tilde{h}_{\mu'}^{\mu} R^{\mu'}{}_{\lambda\alpha'\beta'} v^\lambda \\
&= \left(K_\beta{}^\mu \tilde{h}_\alpha^\rho - K_\alpha{}^\mu \tilde{h}_\beta^\rho \right) \left(\nabla_\rho \left(n_\lambda v^\lambda \right) - v^\lambda \nabla_\rho n_\lambda \right) + \tilde{h}_\alpha^{\alpha'} \tilde{h}_\beta^{\beta'} \tilde{h}_{\mu'}^{\mu} R^{\mu'}{}_{\lambda\alpha'\beta'} v^\lambda \\
&= - \left(K_\beta{}^\mu \tilde{h}_\alpha^\rho - K_\alpha{}^\mu \tilde{h}_\beta^\rho \right) K_{\rho\lambda} v^\lambda + \tilde{h}_\alpha^{\alpha'} \tilde{h}_\beta^{\beta'} \tilde{h}_{\mu'}^{\mu} R^{\mu'}{}_{\lambda\alpha'\beta'} v^\lambda \\
&= \left(\left(K_\alpha{}^\mu \tilde{h}_\beta^\rho - K_\beta{}^\mu \tilde{h}_\alpha^\rho \right) K_{\rho\lambda} + \tilde{h}_\alpha^{\alpha'} \tilde{h}_\beta^{\beta'} \tilde{h}_{\mu'}^{\mu} R^{\mu'}{}_{\lambda\alpha'\beta'} \right) v^\lambda .
\end{aligned} \tag{26}$$

We can then read off the Gauss-Codazzi relation

$$\tilde{R}^{(N-1)\,\mu}{}_{\lambda\alpha\beta} = \left(K_\alpha{}^\mu \tilde{h}_\beta^\rho - K_\beta{}^\mu \tilde{h}_\alpha^\rho \right) K_{\rho\lambda} + \tilde{h}_{\mu'}^{\mu} \tilde{h}_\lambda^{\lambda'} \tilde{h}_\alpha^{\alpha'} \tilde{h}_\beta^{\beta'} R^{\mu'}{}_{\lambda'\alpha'\beta'} . \tag{27}$$

The λ projection in the second term is needed as v, being tangent to the surface, can only probe the tangential information. Taking the trace of the first and third indices of (2.7) creates

$$\begin{aligned}
\tilde{R}^{(N-1)}{}_{\alpha\beta} &= K K_{\alpha\beta} - K_\beta{}^\lambda K_{\alpha\lambda} + \tilde{h}_\mu^\lambda \tilde{h}_\alpha^{\alpha'} \tilde{h}_\beta^{\beta'} R^\mu{}_{\alpha'\lambda\beta'} \\
&= K K_{\alpha\beta} - K_\beta{}^\lambda K_{\alpha\lambda} + \tilde{h}_\alpha^{\alpha'} \tilde{h}_\beta^{\beta'} \left(R_{\alpha'\beta'} - n^\lambda n_\mu R^\mu{}_{\alpha'\lambda\beta'} \right) .
\end{aligned} \tag{28}$$

The third term can be replaced with the energy momentum tensor using Einstein's equation

$$R_{\mu\nu} = 8\pi G_N \left(T_{\mu\nu} - \frac{1}{N-2} T g_{\mu\nu} \right) - \frac{N-1}{l^2} g_{\mu\nu} \tag{29}$$

and the 4th can be simplified by a second application of the commutation identity of the Riemann tensor

$$\begin{aligned}
\tilde{h}_\alpha^{\alpha'} \tilde{h}_\beta^{\beta'} n^\lambda n_\mu R^\mu{}_{\alpha'\lambda\beta'} &= -\tilde{h}_\alpha^{\alpha'} \tilde{h}_\beta^{\beta'} n^\lambda [\nabla_\lambda, \nabla_{\beta'}] n_{\alpha'} \\
&= -\tilde{h}_\alpha^{\alpha'} \tilde{h}_\beta^{\beta'} n^\lambda \left(\nabla_\lambda K_{\beta'\alpha'} - \nabla_{\beta'} K_{\lambda\alpha'} \right) \\
&= -\tilde{h}_\alpha^{\alpha'} \tilde{h}_\beta^{\beta'} \left(n^\lambda \nabla_\lambda K_{\beta'\alpha'} - \nabla_{\beta'} \left(n^\lambda K_{\lambda\alpha'} \right) + K_{\lambda\alpha'} K_{\beta'}{}^\lambda \right) \\
&= -\tilde{h}_\alpha^{\alpha'} \tilde{h}_\beta^{\beta'} \left(n^\lambda \nabla_\lambda K_{\beta'\alpha'} + K_{\lambda\alpha'} K_{\beta'}{}^\lambda \right) \\
&= - \left(n^\lambda \left(\nabla_\lambda \left(\tilde{h}_\alpha^{\alpha'} \tilde{h}_\beta^{\beta'} K_{\beta'\alpha'} \right) - K_{\alpha'\beta'} \nabla_\lambda \left(\tilde{h}_\alpha^{\alpha'} \tilde{h}_\beta^{\beta'} \right) \right) + K_{\lambda\alpha} K_\beta{}^\lambda \right) \\
&= - \left(n^\lambda \nabla_\lambda K_{\beta\alpha} + K_{\lambda\alpha} K_\beta{}^\lambda \right) .
\end{aligned} \tag{30}$$

The second term in the penultimate line disappears as it can be decomposed into extrinsic curvatures which are orthogonal to the normal vector with which

it is contracted. Replacing the first term of (30), with use of (25), we can then use (28) to write

$$\mathcal{L}_n K_{\alpha\beta} = \tilde{R}^{(N-1)}{}_{\alpha\beta} + 2K_\alpha{}^\lambda K_{\beta\lambda} - 8\pi G_N \tilde{h}_\alpha^{\alpha'} \tilde{h}_\beta^{\beta'} T_{\alpha'\beta'} + \left(\frac{N-1}{l^2} + \frac{8\pi G_N}{N-2} T \right) \tilde{h}_{\alpha\beta}. \tag{31}$$

Thus, if we posit that there exists a infinitesimal surface of non zero energy momentum, we can treat $T_{\alpha\beta}$ as the distribution $\delta(z)T_{\alpha\beta}$. Integrating z from $(-\epsilon, \epsilon)$, under the reasonable assumption of a finite discontinuity for all other terms, we find in the limit as ϵ tends to 0

$$K_{\alpha\beta}(z = 0^+) - K_{\alpha\beta}(z = 0^-) = 8\pi G_N \left(\frac{1}{N-2} T \tilde{h}_{\alpha\beta} - \tilde{h}_\alpha^{\alpha'} \tilde{h}_\beta^{\beta'} T_{\alpha'\beta'} \right) \tag{32}$$

which constitute the Israel junction conditions.